Yarmouk University

Hijjawi Faculty for Engineering Technology

A Thesis Submitted to the Department of
Electrical Power Engineering
In Partial Fulfillment of the Requirements for the Degree of
Master of Science

"Highly Penetrated Photovoltaic Generator Integrated to the Power System with Maximum Power Point Tracking Using Perturbation and Observation Algorithm "

Prepared by:

Tha'er Omar Adel Sweidan 2012979019

Advisor:

Prof. Mohammed Bashir Rifai

Co Advisor:

Dr. Mohammad Saleh Widyan

August,2015

Highly Penetrated Photovoltaic Generator Integrated to the Power System with Maximum Power Point Tracking Using Perturbation and Observation Algorithm

BY

Tha'er Omar Adel Sweidan 2012979019

B.sc.Electrical Engineering ,Hashemite University,2011

A Thesis Submitted In Partial Fulfillment of the Requirements for the Degree of
Master of Science in the Department of
Electrical Power Engineering, Yarmouk University, Irbid , Jordan

APPROVED BY

Dr. Mohammed Bashir Rifai...Chairman
Professor of Electrical Power Engineering ,Yarmouk University.

Dr. Ahmad Mohammed Harb...Member
Professor of Electrical Power Engineering ,German Jordanian University.

Dr. Mohammed Saleh Widyan...Member
Associate Professor of Electrical Power Engineering ,Hashemite University.

Dr. Mohammed Awad Momany...Member
Assistant Professor of Electrical Power Engineering ,Yarmouk University

13th August, 2015

www.manaraa.com

ACKNOLEDGMENTS

I would like to express my thanks and gratitude to Allah, who gave me the ability and the willingness to complete this work successfully.

I would also like to thank my supervisors Prof. Mohammed Bashir Rifai and Dr.Mohammad Saleh Widyan for their guidance, patience, support, comments, and valuable advice.

I sincerely thank Prof. Ahamd M. Harb & Dr. Mohammed A. Momany for their participation in the committee and for their encouragement and useful comments.

Also, I want to thank my parents, my brother, and my sisters for their encouragement at all the times.

Lastly, I want to thank any one from my friends and HU colleagues who gave me a hand or tried to help me to complete this work.

Tha'er O.A.Sweidan

Declaration

Plagiarism is the breach of copyright or using another person's work and pretending that is one's own.

I, Tha'er O. Sweidan, recognize what plagiarism is and I hereby declare that this thesis proposal, which is submitted to the department of electrical power engineering at Hijjawi Faculty for engineering technology, for the partial fulfillment of the requirements for the degree of Master of Science, is my own work.

I have not plagiarized from any source. All references and acknowledgment of sources are given and cited in my proposal. I have used the conventional citation and referencing. Each significant contribution to and quotation in this report from work of other people has been attributed and referenced.

Tha'er O.A.Sweidan

List of Tables

List of Figures

VI

VIII

List of Symbols and Abbreviations

PV	Photovoltaic
MPP	Maximum Power Point for photovoltaic cell/module
V_{OC}	Open circuit Voltage for photovoltaic cell/module
I_{SC}	Short circuit current for photovoltaic cell/module
V_{MP}	Voltage at MPP
I_{MP}	Current at MPP
I_D	Diode Current
R_s	Series resistance for photovoltaic cell
R_{sh}	Shunt Resistance for photovoltaic cell
I_s	Saturation current of the diode.
q	Electron charge = $1.6 * 10^{-19}$ Coulombs.
n	Ideality factor
K	Boltzmann constant = $1.38 * 10^{-23}$ Joule/°K.
T	Temperature on absolute scale °K.
I_{PV}	Photovoltaic output current
FF	Fill Factor for Photovoltaic cell
Pin	Input Power
Pout	Output Power
η	Efficiency
P&O	Perturbation and Observation Algorithm
D	Duty cycle for buck boost converter

ΔD	Duty cycle perturbation
V_{abc}	Voltage in abc sequence
V_{dq0}	Voltage in dq0 sequence
I_{abc}	Current in abc sequence
I_{dq0}	Current in direct ,quadrature and zero frame
K	Matrix K for park transformation
K^{-1}	Inverse for Matrix K
V_{PV}	PV generator operating voltage.
C	Capacitance of the LC filter.
$V_{dC}\&V_{qC}$	d&q axis components of the voltage across the capacitor of LC filter, respectively.
$I_{dPV}\&I_{qPV}$	d-axis & q-axis components of PV generator output current, respectively.
$I_{d}\&I_{q}$	d-axis & q-axis components of the transmission line current, respectively.
L	Inductance of the LC filter.
L_{eq}	Equivalent inductance of the transmission line for pre-fault & post-fault conditions.
R_{eq}	Equivalent resistance of the transmission line for pre-fault & post-fault conditions.
V_{inf}	Infinite bus voltage.
δ_{PV}	Delta-angle of the voltage injected by the PV generator.
δ_{inf}	Delta angle of the infinite bus voltage.
$L_{A},L_{B}\&L_{C}$	Inductances of the transmission line branches for during-fault conditions.
$R_{A}, R_{B}\&R_{C}$	Resistances of the transmission line branches for during-fault conditions.
$I_{cd}\&I_{cq}$	d&q axis components of the current through filter capacitor, respectively.

X

$I_{dC} \& I_{qC}$ d&q axis components of the current in C branch of transmission line during-fault.

ω Synchronous Radian Frequency

I_{PV} DC current output of the PV generator

THD   Total Harmonic Distortion

Table of Contents

Abstract

In most photovoltaic PV generator systems, the maximum power output from PV is the target. There are many Maximum Power Point Tracking (MPPT) techniques such as fractional open circuit voltage, fractional short circuit current, perturbation and observation (P&O), incremental conductance, fuzzy logic controller. In this thesis, perturbation and observation (P&O) algorithm is applied to track the maximum power point of the output characteristic of the photovoltaic generator. The system considered is a photovoltaic generator connected to infinite bus via DC –DC buck boost converter, three phase DC to AC inverter, transformer and two identical transmission lines. Large disturbance stability analysis of PV generator integrated with the grid is investigated. This will be associated with the analysis of the system in direct and quadrature frame (d-q) and therefore the derivation of the nonlinear dynamical mathematical equations for the system in d-q frame is one of the steps in my work. The stability of the proposed system is studied after subjecting symmetrical three-phase to ground fault and following successive step changes in the solar intensities of the PV generator. Perturbation and Observation (P&O) algorithm is used to control the duty ratio of DC-DC buck boost converter to give maximum power output from the PV generator by detecting the location of the operating point on the PV generator and control the value of duty cycle of the DC-DC converter.

Chapter

1

Chapter 1: Introduction

This chapter presents thesis objectives, thesis scope and thesis outline.

1.1 Thesis objectives

The objectives of the thesis can be summarized as the following points:

1. Design a photovoltaic generator and obtain its output characteristics in both actual and per unit quantities.

2. Derive the nonlinear dynamical mathematical equations for the system in d- q stationary reference frame using Park Transformation and apply the perturbation and observation algorithm as maximum power point tracking technique for the PV generator.

3. Study the stability of the proposed System after being subjected to symmetrical three phase to ground fault at one of the parallel transmission lines and obtain the response of the system following successive step changes in the solar intensity levels.

1.2 Thesis scope

In this thesis, large signal stability analysis of highly penetrated photovoltaic generator integrated with the power system is investigated. The study comprises the response of the system at wide range of solar irradiance levels. Symmetrical three phase to ground fault is subjected and the system response is observed. The main contribution of this work is the implementation of the perturbation and observation technique as the maximum power point tracking method.

3

1.3 Thesis Outline

Chapter two presents an overview of photovoltaic systems, how it works, the output characteristics and some relations including the way of connections them to each other. Chapter two also discusses the maximum power point tracking techniques and gives an overview about them and focusing on the perturbation and observation algorithm which is considered as the maximum power point tracking method for the PV generator connected to the grid.

The third chapter concentrates on the literature review on photovoltaic systems especially those studies which interested in studying the stability of the power system incorporated with PV generator, interfacing between photovoltaic generator and the grid, and the methods of tracking the maximum power point of PV generator.

Chapter four describes the system under study in this thesis, it's block and schematic diagrams and its components and it presents full derivation of the system mathematical modeling direct and quadrature frame (d-q) by apply park transformation techniques and the mathematical dynamical equations that represent the system in all cases.

Chapter five presents the photovoltaic generator design in both actual and per unit quantities including the area of photovoltaic modules, the number of solar modules, and the primary cost of the photovoltaic solar power plant. Also this chapter shows the perturbation and observation algorithm how it works, the values of duty cycle and duty cycle perturbations corresponding to the output characteristics of the PV generator at different solar irradiance levels.

4

Chapter five also presents and discusses the results of the system response at different solar illuminations when the system is subjected to a symmetrical three phase to ground fault at the middle of one of the transmission lines, and the response of the system when the PV generator solar irradiance level is step changed.

Chapter six presents the conclusions of this work and future work .

5

Chapter

2

Chapter 2: Photovoltaic System and Maximum Power Point Tracking Techniques

This chapter presents an overview of photovoltaic systems, how it works, the output characteristics and some relations including the way of connections them to each other and discusses the maximum power point tracking techniques focusing on the perturbation and observation algorithm which is considered as the maximum power point tracking method for the PV generator connected to the grid.

2.1 Photovoltaic systems and Output Characteristics:

A photovoltaic system converts sunlight into electricity. The basic device of a photovoltaic system is the photovoltaic cell. Solar cell, which is basically a p-n semiconductor junction directly, converts sunlight energy into electricity. The Photovoltaic cell can be represented by the equivalent circuit shown in Fig.2.1
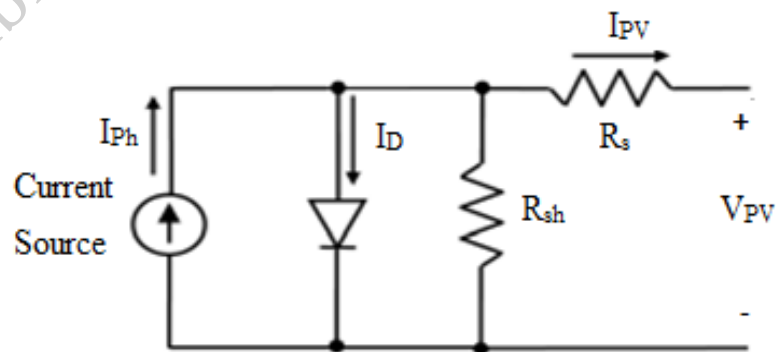
Fig.2.1: Equivalent circuit of photovoltaic cell

The output current of a photovoltaic cell can be mathematically expressed as:

$$I_{PV} = I_{Ph} - I_D - I_{sh} \dots\dots\dots\dots\dots\dots\dots\dots\dots\dots\dots\dots\dots\dots\dots\dots\dots(1)$$

where

I_{PV} : Output photovoltaic current (A).

I_{Ph} : Light generated current (A).

I_D : Diode Current (A).

I_{sh} : Shunt resistance current(A).

The series resistance R_s represents the internal resistance to the current flow, and depends on the p-n junction depth, the impurities and the contact resistance. In an ideal photovoltaic cell, $R_s = 0$ Ω (no series loss), and $R_{sh} = \infty$ Ω (no leakage to ground).The photovoltaic conversion efficiency is sensitive to small variations in R_s, but is insensitive to variations in R_{sh}. A small increase in R_s can decrease the photovoltaic output significantly [1].

The current through these elements is governed by the voltage across them:

$$V_j = V_{PV} + I_{PV} R_S \dots\dots\dots\dots\dots\dots\dots\dots\dots\dots\dots\dots\dots\dots\dots\dots\dots\dots\dots(2)$$

Where

V_j: Voltage across both diode and shunt resistance (V).

V_{PV}: Voltage across the output terminals (V).

R_s: Series resistance (Ω)

8

The diode current is given by the diode current expression:

$$I_D = I_S * \left(\exp\left(\frac{q\,Voc}{nKT}\right) - 1 \right) \dots\dots\dots\dots\dots\dots\dots\dots\dots\dots\dots\dots\dots\dots\dots\dots\dots\dots\dots\dots (3)$$

Where:

I_s = the saturation current of the diode (A).

q = electron charge = $1.6 * 10^{-19}$ (C).

n = ideality factor

K = Boltzmann constant = $1.38 * 10^{-23}$ (J/K).

T = temperature on absolute scale (K).

The load current is given by the expression:

$$Ipv = Iph - Is * \left(\exp\left(\frac{q\,Voc}{nKT}\right) - 1 \right) - \frac{Voc}{Rsh} \dots\dots\dots\dots\dots\dots\dots\dots\dots\dots\dots\dots\dots\dots (4)$$

2.1.1 Open circuit voltage and short circuit current

The most important parameters for describing the cell electrical performance is the open-circuit voltage V_{oc} and the short-circuit current I_{sc}. The short-circuit current is measured by shorting the output terminals of the PV cell , and measuring the terminal current under full illumination.The maximum voltage of the PV cell is the open-circuit voltage. By substituting the PV current in the previous equation with $I_{PV} = 0$ gives the open-circuit voltage as the following [1]:

$$V_{OC} = \frac{nKT}{q} * \log\left(\frac{Iph}{ID} + 1\right) \dots\dots\dots\dots\dots\dots\dots\dots\dots\dots\dots\dots\dots\dots\dots\dots\dots (5)$$

9

2.1.2 Current –Voltage and Power – Voltage characteristics for Photovolatic Cell

The electrical characteristic of the PV cell is generally represented by the current versus voltage (I-V) curve. Figure 2.2 shows the I-V characteristic of a PV module showing the maximum power point (Vmp, Imp) [1] .
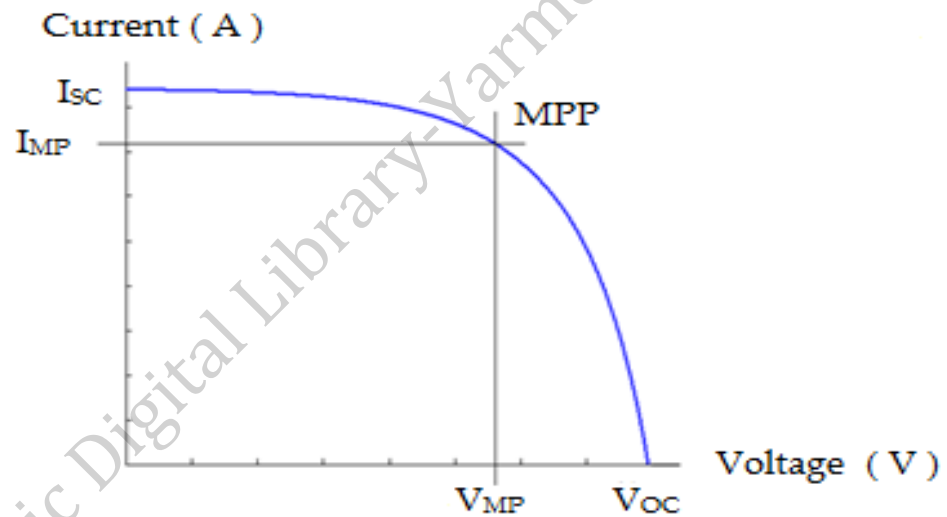
Fig.2.2. I-V Curve of PV Cell

In the above characteristic of the PV cell, the cell works like a constant current source, generating voltage to match the load resistance. The power output of the panel is the product of the voltage and the current outputs. Figure 2.3 shows the power versus voltage indicating the maximum power point MPP of the PV cell. The cell produces the maximum power at voltage corresponding to the knee point of the I-V curve [1].

10
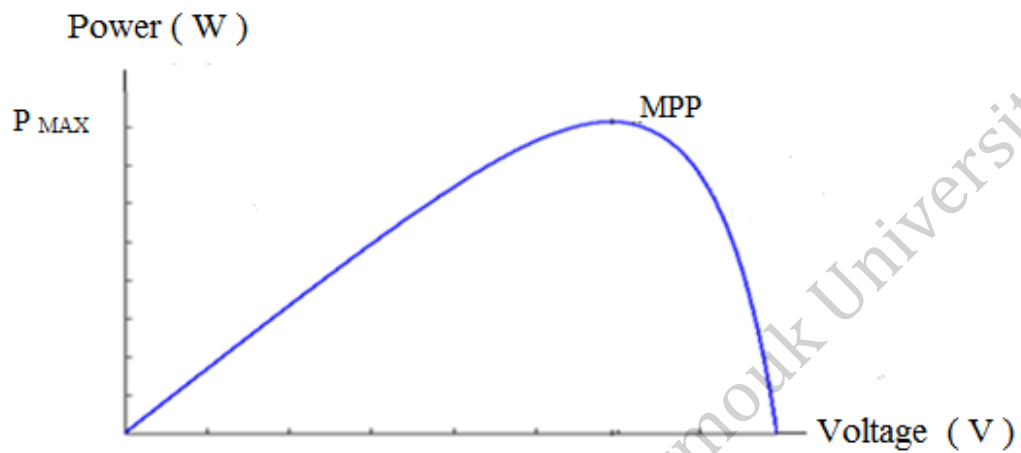
Fig.2.3.The maximum power point of PV cell

2.2 Photovoltaic Fill Factor (FF)

The Fill factor (FF) is a measure of quality of the solar cell. It is calculated by dividing the maximum power to the theoretical power (P_{th}) that would be the product of both the open circuit voltage and short circuit current . In some other words FF is the ratio between the rectangular area with the current voltage characteristic as shown in Fig.2.4 [2].

$$FF = \frac{P_{max}}{P_{th}} = \frac{V_{MP} \cdot I_{MP}}{V_{OC} \, I_{SC}} \dots\dots\dots\dots\dots\dots\dots\dots\dots\dots\dots\dots\dots\dots\dots\dots\dots\dots\dots\dots\dots (6)$$

11
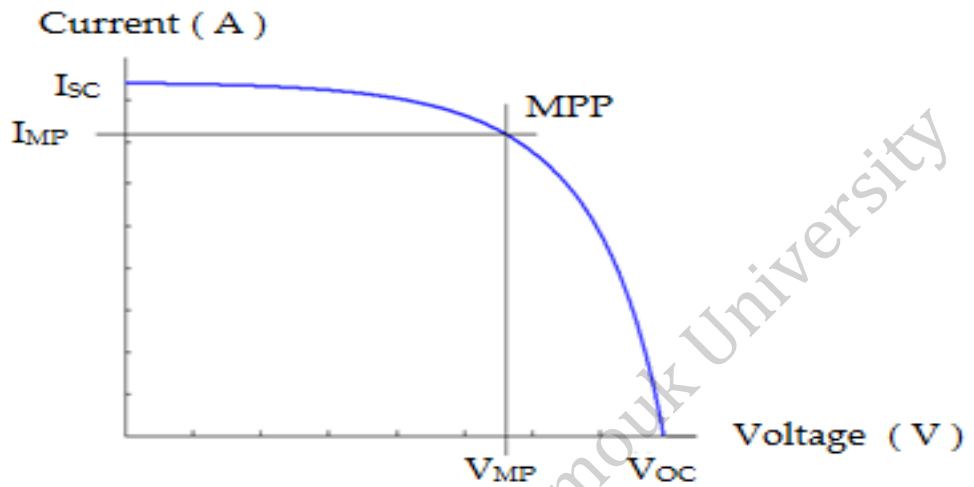
Fig.2.4.Fill factor on I-V Curve

2.3 Photovoltaic Efficiency

Efficiency is the ratio of the electrical power output P_{out} to the solar power input P_{in} into the PV cell. P_{out} can be taken to be P_{max} since the solar cell can be operated up to its maximum power output to get the maximum efficiency

$$\eta = \frac{P_{out}}{P_{in}} \dots\dots\dots\dots\dots\dots\dots\dots\dots\dots\dots\dots\dots\dots\dots\dots\dots\dots\dots(7)$$

$$\eta_{MAX} = \frac{P_{max}}{P_{in}} \dots\dots\dots\dots\dots\dots\dots\dots\dots\dots\dots\dots\dots\dots\dots\dots\dots (8)$$

P_{in} is taken as the product of the irradiance of the incident light, measured in W/m^2 with the surface area of the solar cell [m^2]. The maximum efficiency (η_{MAX}) found from a light test. All of the current and voltage parameters affect by ambient conditions such as temperature and the intensity and spectrum of the incident light[2].

12

2.4 Photovoltaic Layouts:

Cell is the basic element of any photovoltaic system. When the cells are connected together up to 35 cells we call it a module. The solar array is defined as a group of several modules electrically connected in series-parallel combinations to generate the required current and voltage. To increase the current we connect many cells/ modules in parallel combination and connecting it in series to increase voltage of the photovoltaic system as shown in Fig.2.5 [2] .
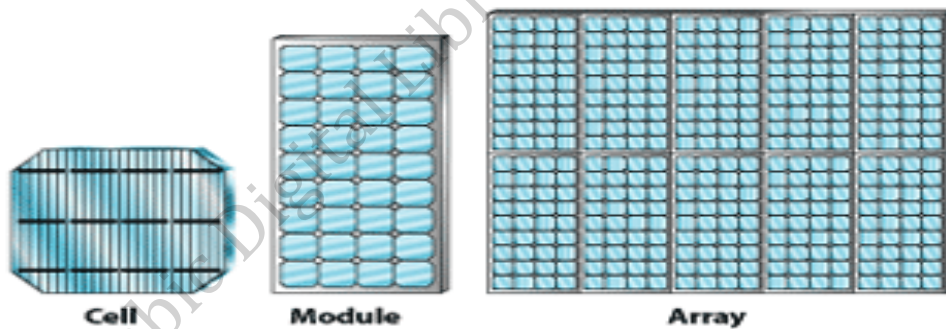
Fig.2.5.Several PV cells make a module and several modules make an array

13

2.5 Types of Photovoltaic Cells

Cells are manufactured from a variety of different types of materials. The most significant is crystalline silicon. There are a broad range of different PV cells produced by over 100 manufacturers. There are 4 main types of commercially available cells: Monocrystalline silicon PV , Polycrystalline silicon PV , Amorphous silicon PV and Hybrid PV. At present monocrystalline PV and polycrystalline PV are the most common and they account for approximately 93% of all modules sold globally in large and small-scale systems. Amorphous silicon accounts for approximately 4.2% of the global market sales. The fourth type of PV cell, is called a hybrid as it consists of a crystalline cell coated in an amorphous layer [3].

1. Monocrystalline Silicon PV

To produce monocrystalline silicon a crystal of silicon is grown from highly pure molten silicon. This single crystal cylindrical ingot is cut into thin slices between 0.2 and 0.3mm thick- this is the basis of a solar PV cell. These PV cells have efficiencies of 13-16 % and are the most efficient type of the three types of silicon PV cell. They require more time and energy to produce than polycrystalline silicon PV cells, and are therefore slightly more expensive[3].

Fig.2.6.Monocrystalline silicon PV module

2. Polycrystalline Silicon PV

Polycrystalline silicon is also produced from a molten and highly pure molten silicon, but using a casting process. The silicon is heated to a high temperature and cooled under controlled conditions as a mould. It sets as an irregular poly- or multi-crystal form. The square silicon block is then cut into 0.3mm slices. The typical blue appearance is due to the application of an anti-reflective layer. The thickness of this layer determines the color- blue has the best optical qualities. It reflects the least and absorbs the most light. More chemical processes and fixing of the conducting grid and electrical contacts complete the process. Mass-produced polycrystalline PV cell modules have an efficiency of 12-16%[3].

Fig.2.7.Polycrystalline silicon PV module

15

3. Amorphous Silicon PV

Amorphous silicon is non-crystalline silicon. Cells made from this material are found in pocket calculators etc. The layer of semi-conductor material is only 0.5-2.0um thick, where 1um is 0.001mm. This means that considerably less raw material is necessary in their production compared with crystalline silicon PV production. The film of amorphous silicon is deposited as a gas on a surface such as glass. Further chemical processes, the fixing of a conducting grid and electrical contacts follow. These PV cells have an efficiency of between 6-8%. Multi-junction amorphous thin film PV cells with each layer sensitive to different wavelengths of the light spectrum are also available. These have slightly higher efficiencies. This type of PV cell is not currently suitable for use on residential developments due to the low generation density[3].
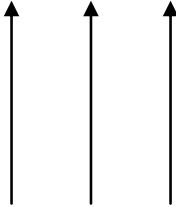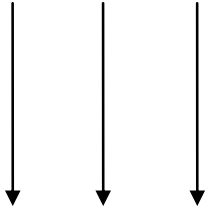
Fig.2.8.Amorphous silicon PV module

4. Hybrid PV

Hybrid photovoltaic cells are classified as PV cells that use two different types of PV technology. The Hybrid PV cell is made by Sanyo and comprises a monocrystalline PV cell covered by an ultra-thin amorphous silicon PV layer. The advantage of these types of cells are that they perform well at high temperatures and maintain higher efficiencies (18%+) than conventional silicon PV cells. However, these cells come at a cost premium[3]. Table 2.1 shows the comparison between three types of photovoltaic with respect to cell's efficiency, energy density and cost .The amorphous silicon PV has lowest efficiency, lowest energy density and highest cost.

Table 2.1: Comparison between PV Cell Types

PV cell Material	PV Module Efficiency (%)	Energy Density (k_{wp}/m^2)	Cost
Hybrid PV	18		
Monocrystalline Silicon PV	13 - 16		
Polycrystalline Silicon PV	12 - 16	↑ ↑ ↑	↓ ↓ ↓
Amorphous Silicon PV	6 - 8		

17

2.6 Maximum Power Point Tracking Techniques

Maximum power point tracking MPPT algorithms are necessary in PV applications because the maximum power point of a solar panel varies with the irradiation and temperature, so the use of MPPT algorithms is required in order to obtain the maximum power from a solar array.

To complete our analysis a simple discussion about the cost of the MPPT technique is presented [4]&[5]. A satisfactory MPPT costs comparison can be carried out by knowing the technique (analogical or digital) adopted in the control device, the number of sensors, and the use of additional power component, considering the other costs (power components, electronic components, boards, etc…) equal for all the devices. To make all the cost comparable between them, the computation cost comparison is formulated taking into account the present spread of MPPT methods. The number of sensors required to implement the MPPT technique also affects the final costs. Most of the time, it is easier and more reliable to measure voltage than current and the current sensors are usually more expensive and bulky. The irradiance or temperature sensors are very expensive and uneconomic.

2.6.1 Fractional Short Circuit Current (FSCC) MPPT

If we examine the I-V curve of a PV module in Fig.2.9, it is evident that the current at MPPT occurs close to the short circuit current. This means that under a given environmental condition if the short circuit current is measured and compared with the photovoltaic current, then an approximated MPPT can be reached[6]. Mathematically, it can be written as:

18

$$I_{MP} = K_1.I_{sc} \quad \text{…………………………………………………………………………....(9)}$$

The constant k_1 can be calculated from the data sheet and typically has a value between 0.8-0.92 [7].
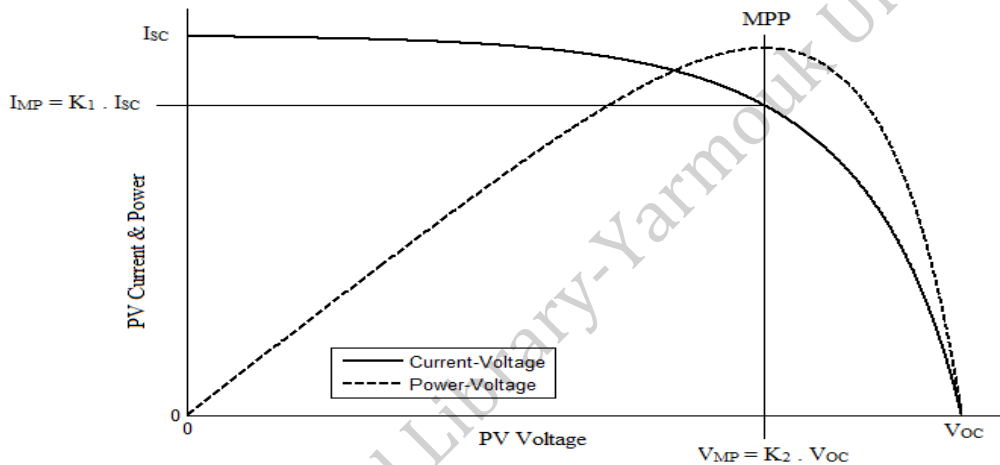
Fig.2.9. I-V&P-V characteristics for FSCC & FOCV

2.6.2 Fractional Open Circuit Voltage (FOCV) MPPT

Similar to the FSCC MPPT , it is observed that the voltage at MPP occurs at a fraction of the OCV as shown in Fig.2.9. Therefore, if we measure V_{OC} and compare it with the photovoltaic voltage, then an approximated maximum power point can be reached. Mathematically, it can be stated as :

$$V_{MP} = K_2.V_{OC} \quad \text{……………………………………………………………………....(10)}$$

The value of k_2 varies from 0.7-0.85 and can be calculated from the datasheet of a particular PV module [7].

19

FOCV and FSCC are called Offline MPPT method .They are worked by disconnecting the PV panel from the system in order to measure either the I_{SC} or V_{OC} (also referred as offline parameters). During the measurement instant, the PV panel is isolated from the rest of the system, hence it is called as offline MPPT[8].

2.6.3 Incremental Conductance Method

The incremental conductance algorithm is based on the fact that the slope of the curve power versus voltage of the PV module is zero at the MPP, positive on the left of it and negative on the right, as can be seen in Fig.2.10 [6].

- $\frac{\Delta P}{\Delta V} = 0$ (At MPP)

- $\frac{\Delta P}{\Delta V} > 0$ (At the right side)

- $\frac{\Delta P}{\Delta V} < 0$ (At the left side)
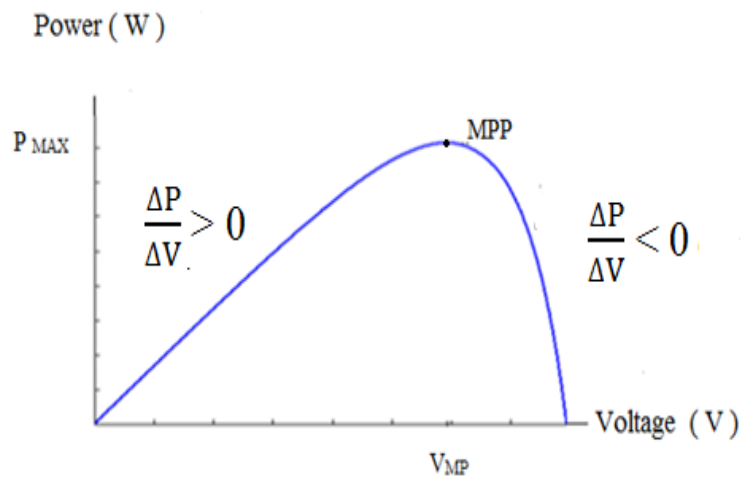
Fig.2.10.Power versus voltage for incremental conductance

20

By comparing the increment of the power vs. the increment of the voltage (current) between two consecutives samples, the change in the MPP voltage can be determined. Algorithm of the Incremental conductance method is shown in Fig.2.11. Similar schemes can be found in [7], [9].
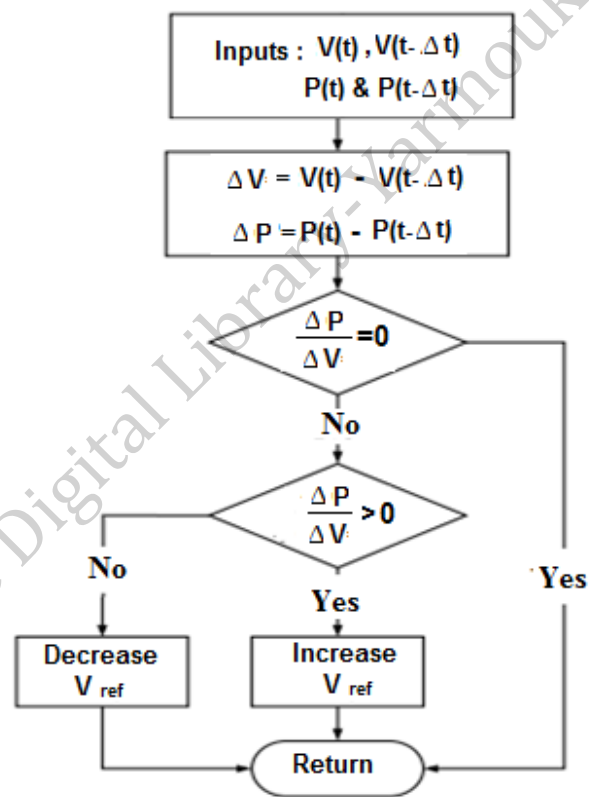
Fig.2.11.Flow chart of incremental conductance

2.6.4 Perturbation and Observation Algorithm (P &O)

Perturbation and observation (P& O) algorithm work by detecting the operating point on the I-V characteristics of the PV array and compare it with the previous operating point. The controller calculate the Power $P(k)=V(k)*I(k)$ at time k and compare it with the previous point $P(k-1)$ and do the action to track the maximum power point by adjusting the duty ratio D of the DC –DC buck- boost converter. This action is fully control by the proposed algorithm [10]. The flow chart of perturbation and observation algorithm is presented in Fig.2.12.
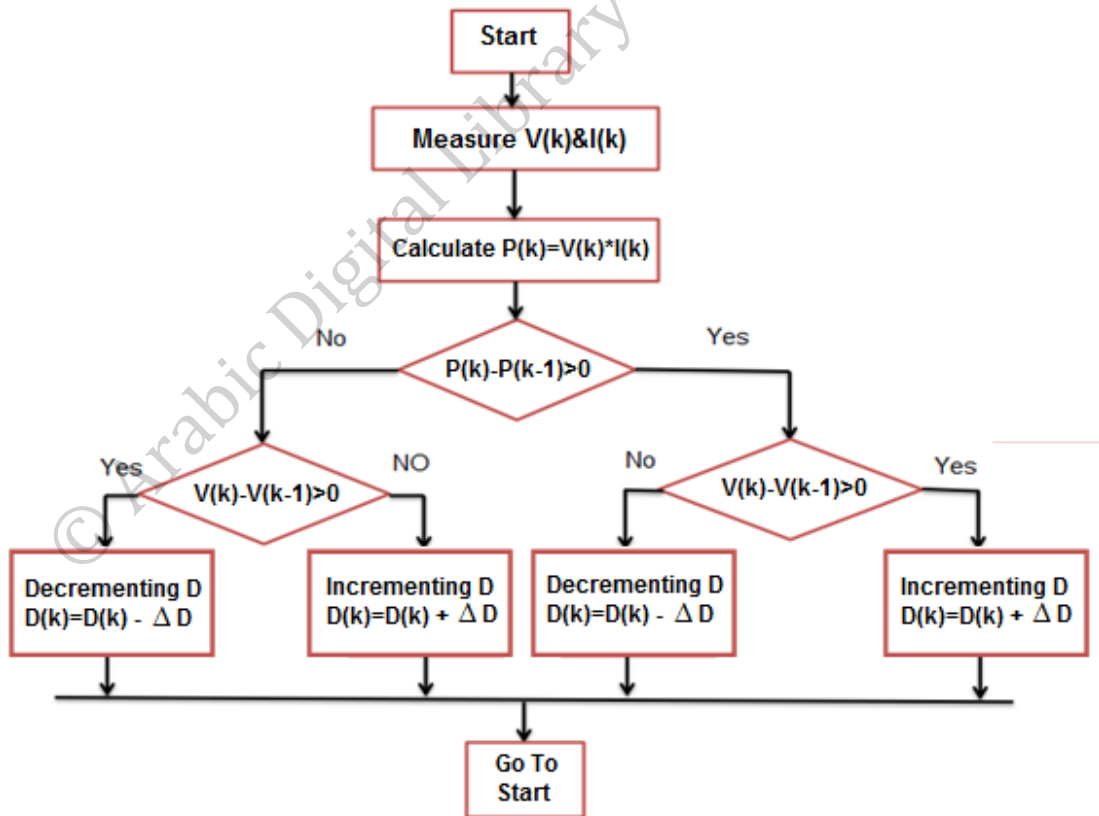
Fig.2.12. Flow Chart of P &O Algorithm

22

If the perturbation of voltage ΔV and power ΔP is positive or even negative, the next duty cycle D perturbation will be positive because the present operating point is located on the left side of the maximum power point. If either one is positive or the other is negative, the next duty cycle perturbation will be negative because the operating point is on the right. Perturbation and observation algorithm alter the duty ratio D of the buck boost convertor to make load matching between photovoltaic and load impedances. Figure 2.13 shows the duty cycle perturbations versus the photovoltaic power-voltage relationship indicating its maximum power point [10].
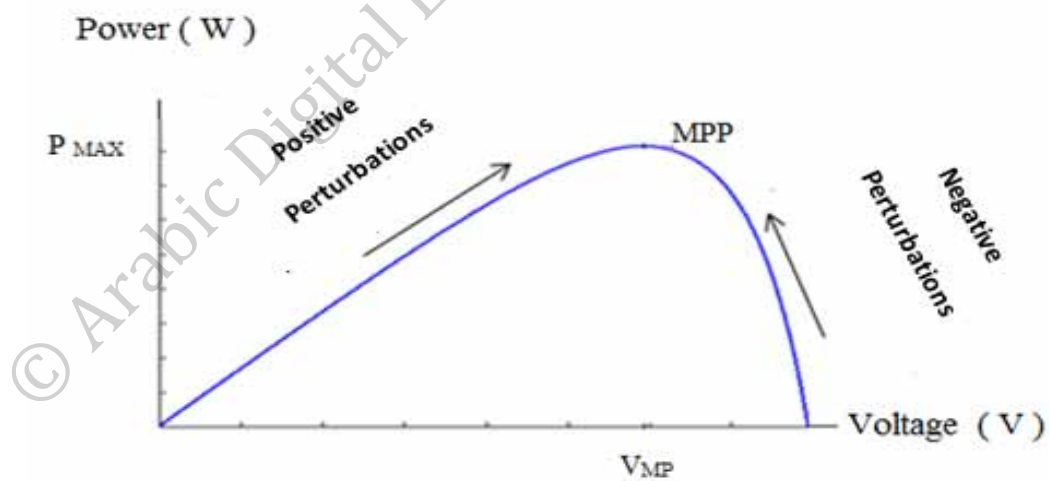
Fig.2.13.Power versus voltage for P & O algorithm

Figure 2.14 illustrates the P and O method. The buck boost converter is used for adjusting the output voltage of PV generator and changing the voltage level up or down from the source voltage. The voltage and current of the PV generator are applied for perturbation and observation while the output provides duty cycle for the buck boost converter. Buck Boost converter controls the output voltage by varying the duty cycle of the switch [11].
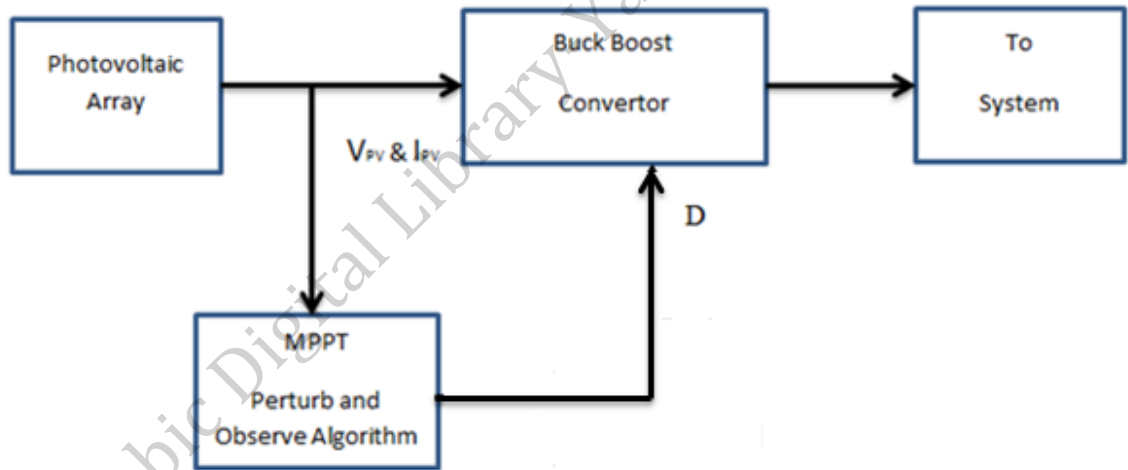
Fig.2.14.Block diagram of P&O MPPT

2.7 DC-DC Buck Boost converter

DC-DC converters are devices used to change the input DC voltage to another level. Buck(step down) converters have an output average voltage equal to or less than the input average voltage. The output voltage of boost converter is equal to or greater than the input average voltage. In DC-DC buck boost converter the average value of the output voltage is higher, equal to, or lower than the input average voltage. They are used in regulated power supplies, motor drive systems and renewable energy systems at intermediate stage for controlling purposes. Buck Boost converter controls the output voltage by varying the duty cycle of the switch D. The circuit for buck-boost converter is shown in Fig.2.15 [12].

Duty ratio D is the ratio between the on state duration of the switch t_{on} and the total and the total switching period T_S.

＊For D>0.5 boost mode, the output voltage is higher than the input voltage.

*For D<0.5 buck mode, the output voltage is lower than the input voltage.

The output voltage of Buck Boost convertor is controlled by duty ratio D.

$$V_O = \frac{D}{1-D} V_{PV} \dots\dots\dots\dots\dots\dots\dots\dots\dots (11)$$

25

The Equivalent circuit of buck boost converter is shown in Fig.2.15.
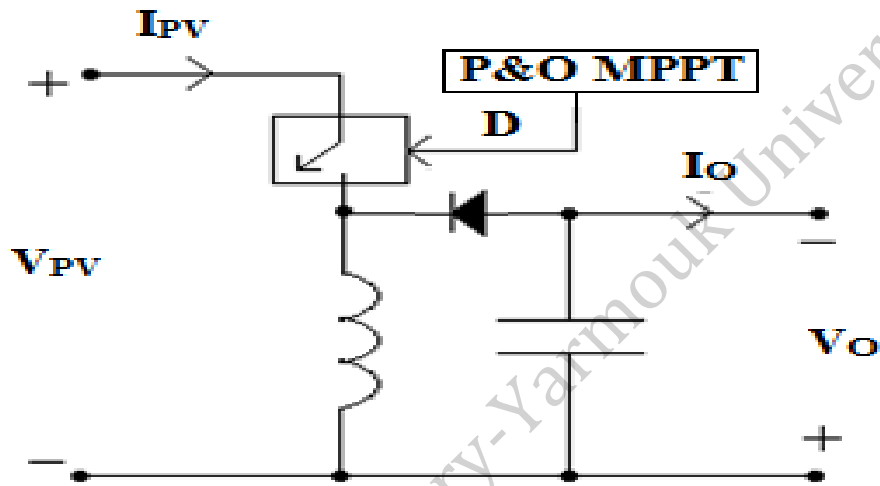
Fig.2.15.Buck-boost converter circuit [12]

Chapter

3

Chapter 3: Literature Review

In [13] the large disturbance stability of grid integrated PV generator is investigated. The MPPT algorithm used is the FOCV method where the running voltage of the PV generator should be in the range of 0.70 – 0.8 of its open circuit voltage. The V_{OC} of the PV generator is measured during the off state of the D.C – D.C converter switch. The system considered is a PV generator integrated to the grid via D.C to D.C converter; three phase sinusoidal D.C to A.C inverter and L- C filter. The results in [13] show that the system has kept the stability of the operating point despite the symmetrical three phases to ground fault subjected at the middle of one of the transmission lines.

In [14] simulation and analysis of P and O algorithm for PV array is presented. The PV array is connected to load using Ćuk convertor. The system in this paper is simulated using MATLAB/SIMULINK. The P and O algorithm gives the optimum duty cycle as compared with constant duty cycle control to extract the maximum power from the PV panel. The PV system output power increases with rise in solar irradiance and fall in cell temperature.

In [15] the P and O algorithm as maximum power point tracking is carried out. The photovoltaic generator is feeding the AC loads via buck boost DC to DC converter. By varying the duty cycle of the buck boost convertor the impedance matching between source and load is occurred which improves the efficiency of the system.

28

In [16] the operating point stability of single machine connected to infinite bus equipped with high PV penetration is investigated. FOCV method is used as MPPT for PV generator. The nonlinear dynamical mathematical model of synchronous generator in d-q reference frame is used including the dynamics of its damper windings and automatic voltage regulator. The PV generator is connected to the system at the middle of transmission line through DC to DC buck boost convertor, DC to AC inverter and transformer. The response of the system after successive step changes on the synchronous generator mechanical power at three solar intensity levels is carried out and the response of the system after successive step changes on the solar intensities has been outlined. The results showed that the field current of synchronous generator is increased as the solar illumination decreased for a given input mechanical power and for a given solar irradiance level the voltage injected by the PV generator is kept constant in spite of the step changes in the generator input mechanical power. The delta angle of the voltage injected by the PV generator is independent of the PV generator running conditions. It has also indicated that, the power system can withstand higher disturbance values if the power injected by the PV generator increased.

In [17] the design and analysis of P and O algorithm is carried out. This work proposed the design of PV system, simple boost converter, perturbation and observation (P&O) and improved perturbation and observation (IP&O) as maximum power point tracking techniques for the power output from the photovoltaic system. This research compared the results between (P&O) and (IP&O) techniques.

29

In [18] the Comparison of maximum power point tracking algorithms for DC-DC Converters in PV Systems is carried out. This paper presented the comparison between incremental conductance (IC) algorithm and perturbation and observation (P&O) algorithm for tracking the maximum power point from the photovoltaic system using buck converter and boost converter. The simulation for buck convertor and boost converter is done with incremental conductance method and perturbation and observation method. The overall comparison between two MPPT methods is obtained.

In [19] the DC to DC converters for PV generator are designed. The P and O algorithm is used to track the maximum power point for the PV module. The DC to DC convertor is used as interface between PV module and the load to match the maximum power point (MPP) of PV module when climatic conditions change with different resistive load values. The effect of climatic conditions on the design of two components(Inductance , Capacitance) for three types of DC to DC converters(buck ,boost and buck-boost) are taken into consideration . The design of these convertors is based on two principles. For a steady-state operation in a continuous conduction mode, the inductance value for all choppers must be greater than the maximum value of boundary inductance, and in order to limit the output voltage ripple of DC-DC converter below a desired value, the filter capacitance must be larger than the maximum value of boundary capacitance.

In [20] the analysis of a standalone PV system with reduced switch cascaded multilevel inverter is presented. a photovoltaic (PV) system with single phase multilevel inverter (MLI) feeding standalone loads. The system consists of PV array,

30

DC-DC boost converter with maximum power point tracking (MPPT) controller and a reduced switch cascaded inverter. The proposed MLI is advantageous in terms of performance and efficiency as it minimizes switching losses which are prevalent in the conventional cascaded one. The non-linear nature of the PV array is combated by a DC-DC converter which is controlled by P and O MPPT algorithm. The performance of the proposed system is verified through a simulation study in MATLAB/Simulink and also by developing a prototype of 200 watts. The simulation and hardware results demonstrate minimal switching losses, low THD value with increased DC utilization suitable for various standalone household loads.

In [21] the large-and small-signal stability analysis of a power system incorporated with PV generator is investigated. The PV generator is designed such that the power delivered at MPP at full solar illumination is about 0.65 pu. The study is carried out at different solar illuminations and compared with the case of no PV generation. A DC–DC buck–boost switch mode converter is used at the terminals of the PV array to keep the constant injected voltage at different realistic solar illuminations. The dynamic response of the delta angle of the PV generating bus is extracted. The results show that injecting power from PV panels improves the dynamic stability of the power system. All of the numerical simulations are executed via MATLAB TM software environment by building the code required.

Chapter

4

Chapter 4: System Design and Dynamical Mathematical Model

This chapter presents the system under study its components and how its connected and the full detailed for the derivation of the nonlinear dynamical mathematical model of the system in direct and quadrature frame.

4.1 System under Study

The proposed system includes PV generator with buck boost D.C to D.C convertor and three phase D.C to A.C Inverter and L-C filter that eliminate the unwanted harmonics. Three phase step up transformer is used to connect PV generator to infinite bus via two identical transmission lines. In stability studies, the system should be studied under direct and quadrature frame.

Power system transient stability problem relates to the ability of the power system to keep the stability of the operating point after relatively big disturbance takes place on vital transmission line or any power system component. Example of these disturbances is symmetrical three-phase to ground fault which is consider as a big disturbance that affect on the system stability. Figure 4.1 presents the schematic diagram of the proposed system showing all components.

33
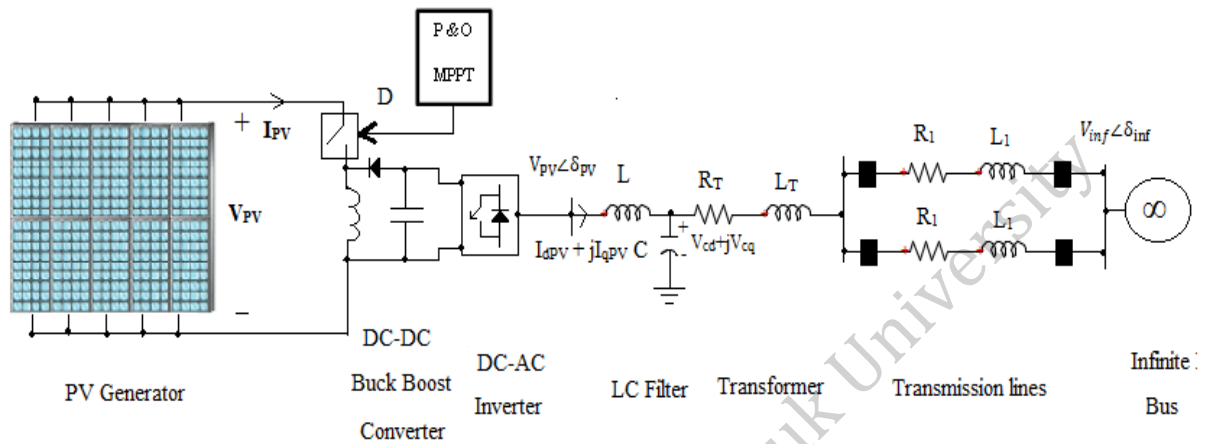
Fig.4.1.Schematic diagram for the power system under study

The nonlinear differential equation of the system is derived and converted to direct and quadrature frame (d-q) using park transformation techniques. Under balanced conditions the zero components for dq0 transformations equal zero. The following equations used to convert any abc system to d-q system[22]

$$V_{dq0} = K\, V_{abc} \dots\dots\dots\dots\dots\dots\dots\dots\dots\dots\dots\dots\dots\dots\dots\dots\dots\dots (12)$$

$$I_{dq0} = K\, I_{abc} \dots\dots\dots\dots\dots\dots\dots\dots\dots\dots\dots\dots\dots\dots\dots\dots\dots\dots (13)$$

$$V_{abc} = K^{-1} V_{dq0} \dots\dots\dots\dots\dots\dots\dots\dots\dots\dots\dots\dots\dots\dots\dots\dots (14)$$

$$I_{abc} = K^{-1} I_{dq0} \qquad \dots\dots\dots\dots\dots\dots\dots\dots\dots\dots\dots\dots\dots\dots\dots (15)$$

where K , K^{-1} and $K^{-1}.\dfrac{dK}{dt}$ are matrices used to complete the park transformation

$$K = \frac{2}{3}\begin{bmatrix} \cos\theta & \cos(\theta-120) & \cos(\theta+120) \\ \sin\theta & \sin(\theta-120) & \sin(\theta+120) \\ \frac{1}{2} & \frac{1}{2} & \frac{1}{2} \end{bmatrix} \qquad \dots\dots\dots\dots\dots\dots\dots\dots\dots\dots (16)$$

34

The Inverse for Matrix K is

$$K^{-1} = \begin{bmatrix} \cos\theta & \sin\theta & 1 \\ \cos(\theta-120) & \sin(\theta-120) & 1 \\ \cos(\theta+120) & \sin(\theta+120) & 1 \end{bmatrix} \quad \text{.. (17)}$$

The product between K^{-1} and the derivative of K is

$$K^{-1} \cdot \frac{dK}{dt} = \begin{bmatrix} 0 & -\omega & 0 \\ \omega & 0 & 0 \\ 0 & 0 & 0 \end{bmatrix} \quad \text{....…..…………..(18)}$$

35

4.2 Mathematical Model of the System for the Pre-Fault Running Conditions:

The derivation of the nonlinear dynamical mathematical equations for the system under study at pre fault running condition
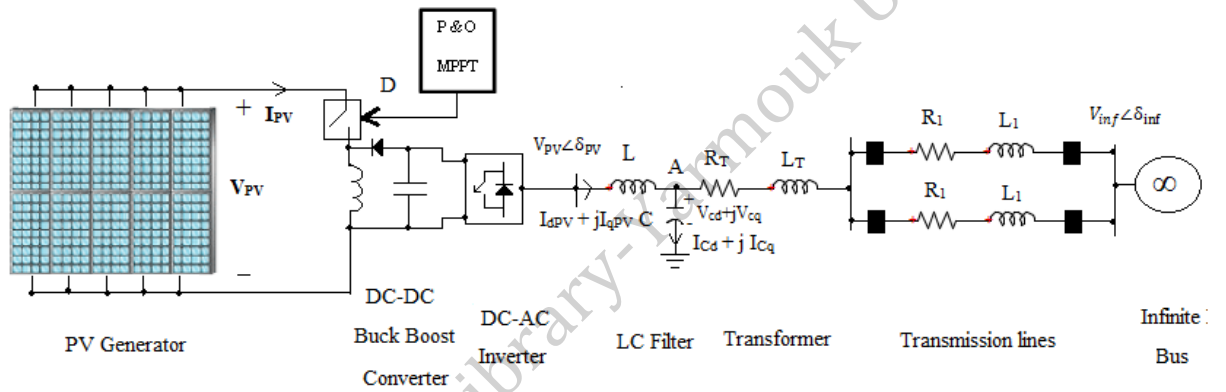
Fig.4.2.Schematic diagram for the pre-fault power system under study

The system can be simplified by taking the two parallel transmission lines and series transformer resistances and inductances are equivalent to R_{eq} & L_{eq}
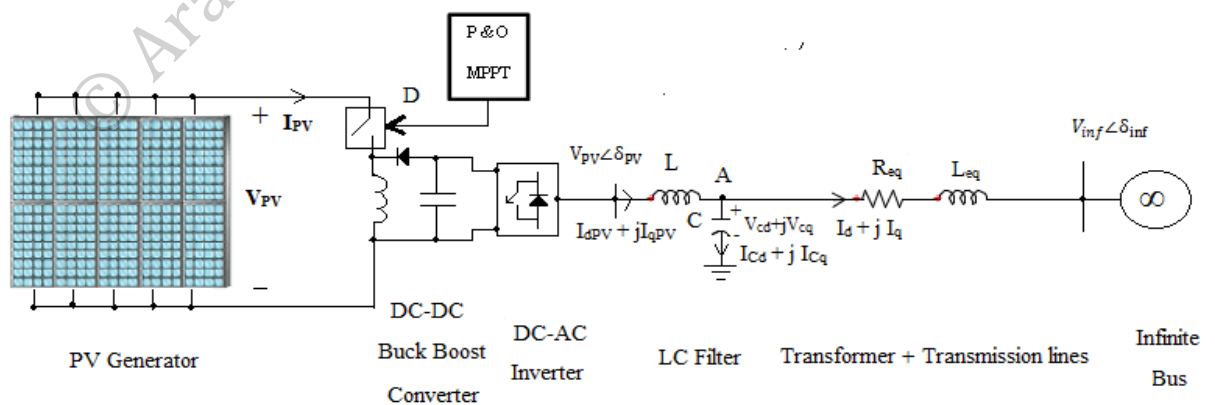
Fig.4.3.Simplified schematic diagram for the pre-fault power system under study

© Arabic Digital Library-Yarmouk University

www.manaraa.com

For LC Filter

The Current in the capacitor of the LC filter is given following equation[22]

$$Ic_{abc} = C \frac{dV_{C_{abc}}}{dt} \quad\text{...(19)}$$

Multiply both sides by K^{-1}

$$K^{-1}. Ic_{dq\,0} = C \frac{dK^{-1}.V_{C_{dq\,0}}}{dt} \quad\text{..(20)}$$

Multiply both sides by K to eliminate the K^{-1} from the left side as follows

$$K. K^{-1}. Ic_{dq\,0} = K. C \frac{dK^{-1}.V_{C_{dq\,0}}}{dt} \quad\text{...(21)}$$

The current through the capacitance of the LC filter in dq0 frame is:

$$Ic_{dq\,0} = K. C \frac{dK^{-1}.V_{C_{dq\,0}}}{dt} \quad\text{..(22)}$$

Do the derivation of the right side and re arrange equations and substituting the park transformation matrices

$$Ic_{dq\,0} = K. C \left(\frac{dK^{-1}}{dt}. V_{C_{dq\,0}} + K^{-1}. \frac{dV_{C_{dq\,0}}}{dt} \right) \quad\text{...(23)}$$

$$Ic_{dq\,0} = C \left(K. \frac{dK^{-1}}{dt}. V_{C_{dq\,0}} + K. K^{-1}. \frac{dV_{C_{dq\,0}}}{dt} \right) \quad\text{..(24)}$$

$$Ic_{dq\,0} = \begin{bmatrix} C & 0 & 0 \\ 0 & C & 0 \\ 0 & 0 & C \end{bmatrix} \begin{bmatrix} 0 & -\omega & 0 \\ \omega & 0 & 0 \\ 0 & 0 & 0 \end{bmatrix} \begin{bmatrix} V_{Cd} \\ V_{Cq} \\ V_{C0} \end{bmatrix} + \begin{bmatrix} C & 0 & 0 \\ 0 & C & 0 \\ 0 & 0 & C \end{bmatrix} \frac{d}{dt} \begin{bmatrix} V_{Cd} \\ V_{Cq} \\ V_{C0} \end{bmatrix}$$

37

2.Apply KCL at node A

$$Ic_d = I_{dPV} - I_d \dotfill (25)$$

$$Ic_q = I_{qPV} - I_q \dotfill (26)$$

So rearrange the above equation and in per unit $\omega = 1$

$$C\frac{dV_{Cd}}{dt} = I_{dPV} - I_d + CV_{Cq} \dotfill (27)$$

$$C\frac{dV_{Cq}}{dt} = I_{qPV} - I_q - CV_{Cd} \dotfill (28)$$

2.Apply KVL around the loop which contains the inductance and capacitance of the LC filter

$$\frac{D}{1-D}V_{PV} \angle \delta_{PV} = L\frac{dI_{PVabc}}{dt} + V_{C_{abc}} \dotfill (29)$$

Substituting each abc variable to its dq0 equivalent by multiplying both sides by K^{-1}

$$K^{-1}\frac{D}{1-D}V_{PV} \angle \delta_{PV} = L\frac{dK^{-1}.I_{PVdq\,0}}{dt} + K^{-1}V_{C_{dq\,0}} \dotfill (30)$$

Multiply both sides by K to eliminate the K^{-1} from the left side

$$K.K^{-1}\frac{D}{1-D}V_{PV} \angle \delta_{PV} = LK.\frac{dK^{-1}.I_{PVdq\,0}}{dt} + K.K^{-1}V_{C_{dq\,0}} \dotfill (31)$$

$$\frac{D}{1-D}V_{PV} \angle \delta_{PV} = LK.\frac{dK^{-1}.I_{PVdq\,0}}{dt} + V_{C_{dq\,0}} \dotfill (32)$$

Do the derivation of the right side and re arrange equations and substituting the park transformation matrices

38

$$\frac{D}{1-D} V_{PV} \angle \delta_{PV} = L(K. \frac{dK^{-1}}{dt} I_{PVdq\,0} + KK^{-1} \frac{dI_{PVdq\,0}}{dt}) + V_{C_{dq\,0}} \dots\dots\dots\dots\dots\dots\dots\dots\dots(33)$$

$$\frac{D}{1-D} V_{PV} \angle \delta_{PV} = \begin{bmatrix} L & 0 & 0 \\ 0 & L & 0 \\ 0 & 0 & L \end{bmatrix} \begin{bmatrix} 0 & -\omega & 0 \\ \omega & 0 & 0 \\ 0 & 0 & 0 \end{bmatrix} \begin{bmatrix} I_{dPV} \\ I_{qPV} \\ V_{I_0PV} \end{bmatrix} + \begin{bmatrix} L & 0 & 0 \\ 0 & L & 0 \\ 0 & 0 & L \end{bmatrix} \frac{d}{dt} \begin{bmatrix} I_{dPV} \\ I_{qPV} \\ I_{0PV} \end{bmatrix} + \begin{bmatrix} V_{Cd} \\ V_{Cq} \\ V_{C0} \end{bmatrix}$$

$$L \frac{dI_{dPV}}{dt} = \frac{D}{1-D} V_{PV} \sin(\delta_{PV}) + LI_{qPV} - V_{Cd} \dots\dots\dots\dots\dots\dots\dots\dots\dots\dots\dots\dots\dots\dots\dots(34)$$

$$L \frac{dI_{qPV}}{dt} = \frac{D}{1-D} V_{PV} \cos(\delta_{PV}) - LI_{dPV} - V_{Cq} \dots\dots\dots\dots\dots\dots\dots\dots\dots\dots\dots\dots\dots\dots(35)$$

3. Apply KVL around the loop which contains capacitor ,transformer and transmission lines ending with infinite bus

$$V_{C_{abc}} = R_{eq} I_{abc} + L_{eq} \frac{dI_{abc}}{dt} + V_{infabc} \angle \delta_{inf} \dots\dots\dots\dots\dots\dots\dots\dots\dots\dots\dots\dots\dots(36)$$

Multiply both sides by K^{-1}

$$K^{-1} V_{C_{dq\,0}} = R_{eq} K^{-1} I_{dq\,0} + L_{eq} \frac{dK^{-1}I_{dq\,0}}{dt} + K^{-1} V_{inf} \angle \delta_{inf} \dots\dots\dots\dots\dots\dots\dots\dots(37)$$

Multiply both sides by K to eliminate the K^{-1} from the left side

$$K. K^{-1} V_{C_{dq\,0}} = R_{eq} K. K^{-1} I_{dq\,0} + L_{eq} K. \frac{dK^{-1}I_{dq\,0}}{dt} + K. K^{-1} V_{inf} \angle \delta_{inf} \dots\dots\dots\dots\dots(38)$$

$$V_{C_{dq\,0}} = R_{eq} I_{dq\,0} + L_{eq} K. \frac{dK^{-1}.I_{dq\,0}}{dt} + V_{inf} \angle \delta_{inf} \dots\dots\dots\dots\dots\dots\dots\dots\dots\dots\dots\dots\dots(39)$$

by derivation the right side and rearrange equations and substituting the park transformation matrices

$$V_{C_{dq\,0}} = R_{eq} I_{dq\,0} + L_{eq} K. (I_{dq\,0} \frac{dK^{-1}}{dt} + K^{-1} \frac{dI_{dq\,0}}{dt}) + V_{inf} \angle \delta_{inf} \dots\dots\dots\dots\dots\dots\dots(40)$$

39

$$V_{C_{dq0}} = R_{eq} I_{dq0} + L_{eq}(K.\frac{dK^{-1}}{dt}I_{dq0} + K.K^{-1}\frac{dI_{dq0}}{dt}) + V_{inf}\angle\delta_{inf} \dots\dots\dots\dots\dots\dots\dots\dots\dots(41)$$

$$\begin{bmatrix} V_{Cd} \\ V_{Cq} \\ V_{C0} \end{bmatrix} = \begin{bmatrix} R_{eq} & 0 & 0 \\ 0 & R_{eq} & 0 \\ 0 & 0 & R_{eq} \end{bmatrix}\begin{bmatrix} I_d \\ I_q \\ I_0 \end{bmatrix} + \begin{bmatrix} L_{eq} & 0 & 0 \\ 0 & L_{eq} & 0 \\ 0 & 0 & L_{eq} \end{bmatrix}\begin{bmatrix} 0 & -\omega & 0 \\ \omega & 0 & 0 \\ 0 & 0 & 0 \end{bmatrix}\begin{bmatrix} I_d \\ I_q \\ I_0 \end{bmatrix}$$

$$+ \begin{bmatrix} L_{eq} & 0 & 0 \\ 0 & L_{eq} & 0 \\ 0 & 0 & L_{eq} \end{bmatrix}\frac{d}{dt}\begin{bmatrix} I_d \\ I_q \\ I_0 \end{bmatrix} + V_{inf}\angle\delta_{inf}$$

$$L_{eq}\frac{dI_d}{dt} = V_{Cd} - R_{eq}I_d + L_{eq}I_q - V_{inf}\sin(\delta_{inf}) \dots\dots\dots\dots\dots\dots\dots\dots\dots\dots\dots\dots\dots(42)$$

$$L_{eq}\frac{dI_q}{dt} = V_{Cq} - R_{eq}I_q - L_{eq}I_d - V_{inf}\cos(\delta_{inf}) \dots\dots\dots\dots\dots\dots\dots\dots\dots\dots\dots\dots\dots(43)$$

From equations 23- 26 ,the delta angle for the PV injected voltage bus is

$$\tan(\delta_{PV}) = \frac{-LI_{q\,PV} + V_{Cd}}{LI_{d\,PV} + V_{Cq}} = \frac{-LI_{q\,PV} + R_{eq}I_d - L_{eq}I_q}{LI_{d\,PV} + R_{eq}I_q + L_{eq}I_d + V_{inf}\cos(\delta_{inf})} \qquad \dots\dots\dots\dots\dots\dots\dots\dots(44)$$

The magnitude of the PV current is

$$I_{PV} = \sqrt{I_{dPV}{}^2 + I_{qPV}{}^2} \dots\dots\dots\dots\dots\dots\dots\dots\dots\dots\dots\dots\dots\dots\dots\dots\dots\dots\dots\dots\dots\dots(45)$$

40

4.3 Mathematical Model of the System for the During Fault Running Conditions:

The derivation of the nonlinear dynamical mathematical equations for the system under study during fault:
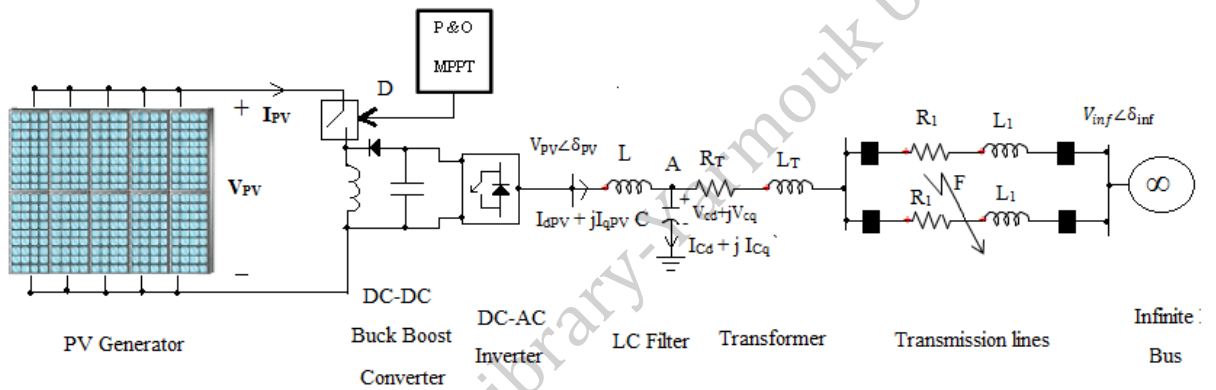
Fig.4.4.Schematic diagram for the during fault power system under study
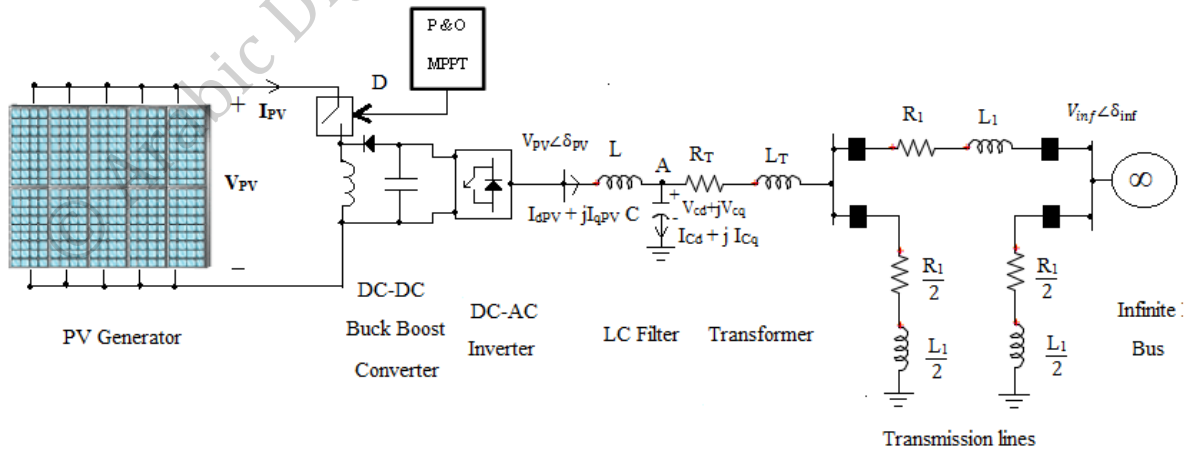
Fig.4.5.Equivalent schematic diagram for the during fault power system under study

After converting the system from Delta to Star
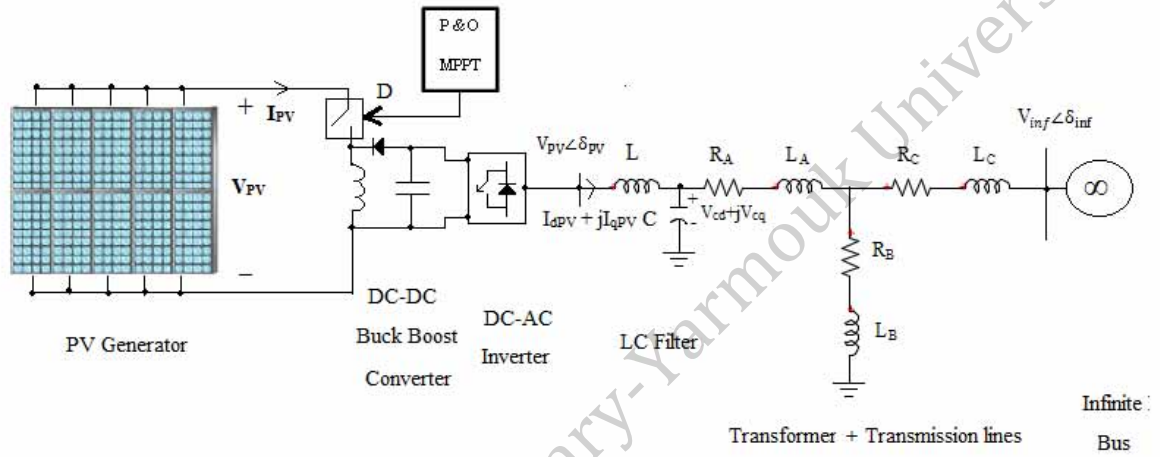
Fig.4.6. Simplified schematic diagram for the during fault power system under study

Apply KVL around the loop which contains the inductance and capacitance of the LC filter

$$\frac{D}{1-D}V_{PV} \angle \delta_{PV} = L\frac{dI_{PVabc}}{dt} + V_{C_{abc}} \dots\dots\dots\dots\dots\dots\dots\dots\dots\dots\dots\dots\dots(46)$$

Substituting each abc variable to its dq0 equivalent by multiplying both sides by K^{-1}

$$K^{-1}\frac{D}{1-D}V_{PV} \angle \delta_{PV} = L\frac{dK^{-1}.I_{PV\ dq\ 0}}{dt} + K^{-1}V_{C_{dq\ 0}} \dots\dots\dots\dots\dots\dots\dots\dots\dots\dots\dots(47)$$

Multiply both sides by K to eliminate the K^{-1} from the left side

$$K.K^{-1}\frac{D}{1-D}V_{PV} \angle \delta_{PV} = LK.\frac{dK^{-1}.I_{PVdq\ 0}}{dt} + K.K^{-1}V_{C_{dq\ 0}} \dots\dots\dots\dots\dots\dots\dots\dots\dots(48)$$

42

$$\frac{D}{1-D}V_{PV}\angle\delta_{PV} = LK.\frac{dK^{-1}.I_{PVdq\,0}}{dt} + V_{C_{dq\,0}} \quad\text{...(49)}$$

Do the derivation of the right side and re arrange equations and substituting the park transformation matrices

$$\frac{D}{1-D}V_{PV}\angle\delta_{PV} = L(K.\frac{dK^{-1}}{dt}I_{PVdq\,0} + KK^{-1}\frac{dI_{PVdq\,0}}{dt}) + V_{C_{dq\,0}} \quad\text{.............................(50)}$$

$$\frac{D}{1-D}V_{PV}\angle\delta_{PV} = \begin{bmatrix} L & 0 & 0 \\ 0 & L & 0 \\ 0 & 0 & L \end{bmatrix}\begin{bmatrix} 0 & -\omega & 0 \\ \omega & 0 & 0 \\ 0 & 0 & 0 \end{bmatrix}\begin{bmatrix} I_{dPV} \\ I_{qPV} \\ V_{I_{0PV}} \end{bmatrix} + \begin{bmatrix} L & 0 & 0 \\ 0 & L & 0 \\ 0 & 0 & L \end{bmatrix}\frac{d}{dt}\begin{bmatrix} I_{dPV} \\ I_{qPV} \\ I_{0PV} \end{bmatrix} + \begin{bmatrix} V_{Cd} \\ V_{Cq} \\ V_{C0} \end{bmatrix}$$

$$L\frac{dI_{dPV}}{dt} = \frac{D}{1-D}V_{PV}\sin(\delta_{PV}) + LI_{qPV} - V_{Cd} \quad\text{...(51)}$$

$$L\frac{dI_{qPV}}{dt} = \frac{D}{1-D}V_{PV}\cos(\delta_{PV}) - LI_{dPV} - V_{Cq} \quad\text{...(52)}$$

Apply KVL around the loop from filter's capcitance C through branches A and B

$$V_{C_{abc}} = R_A I_{A_{abc}} + L_A \frac{dI_{A_{abc}}}{dt} + R_B I_{B_{abc}} + L_B \frac{dI_{B_{abc}}}{dt} \quad\text{...(53)}$$

But

$$I_{B_{abc}} = I_{A_{abc}} - I_{C_{abc}} \quad\text{...(54)}$$

Substituting each abc variable to its dq0 equivalent by multiplying both sides by K⁻

$$K^{-1}V_{C_{dq\,0}} = R_A K^{-1}I_{A_{dq\,0}} + L_A \frac{dK^{-1}I_{A_{dq\,0}}}{dt} + R_B\left(K^{-1}I_{A_{dq\,0}} - K^{-1}I_{C_{dq\,0}}\right) +$$

$$L_B(\frac{dK^{-1}I_{A_{dq\,0}}}{dt} - \frac{dK^{-1}I_{C_{dq\,0}}}{dt}) \quad\text{...(55)}$$

Multiply both sides by K to eliminate the K⁻¹ from the left side

43

$$K.K^{-1}V_{C_{dq\,0}} = R_A K.K^{-1}I_{A_{dq\,0}} + L_A K.\frac{dK^{-1}I_{A_{dq\,0}}}{dt} + R_B\left(K.K^{-1}I_{A_{dq\,0}} - K.K^{-1}I_{C_{dq\,0}}\right) +$$

$$L_B K.\left(\frac{dK^{-1}I_{A_{dq\,0}}}{dt} - \frac{dK^{-1}I_{C_{dq\,0}}}{dt}\right) \dots\dots\dots\dots\dots\dots\dots\dots\dots\dots\dots\dots\dots\dots\dots\dots\dots(56)$$

$$V_{C_{dq\,0}} = R_A I_{A_{dq\,0}} + L_A K.\frac{dK^{-1}I_{A_{dq\,0}}}{dt} + R_B\left(I_{A_{dq\,0}} - I_{C_{dq\,0}}\right) + L_B K.\left(\frac{dK^{-1}I_{A_{dq\,0}}}{dt} - \right.$$

$$\left.\frac{dK^{-1}I_{C_{dq\,0}}}{dt}\right)\dots\dots\dots\dots\dots\dots\dots\dots\dots\dots\dots\dots\dots\dots\dots\dots\dots\dots\dots\dots\dots\dots\dots\dots(57)$$

by derivation the right side and rearrange equations and substituting the park transformation matrices

$$V_{C_{dq\,0}} = R_A I_{A_{dq\,0}} + L_A K.\left(I_{A_{dq\,0}}\frac{dK^{-1}}{dt} + K^{-1}\frac{dI_{A_{dq\,0}}}{dt}\right) + R_B\left(I_{A_{dq\,0}} - I_{C_{dq\,0}}\right) + L_B K.\left(I_{A_{dq\,0}}\frac{dK^{-1}}{dt} + \right.$$

$$\left.K^{-1}\frac{dI_{A_{dq\,0}}}{dt}\right) - \left(I_{C_{dq\,0}}\frac{dK^{-1}}{dt} + K^{-1}\frac{dI_{C_{dq\,0}}}{dt}\right)\dots\dots\dots\dots\dots\dots\dots\dots\dots\dots\dots\dots\dots\dots\dots(58)$$

$$V_{C_{dq\,0}} = R_A I_{A_{dq\,0}} + L_A\left(I_{A_{dq\,0}}K.\frac{dK^{-1}}{dt} + K.K^{-1}\frac{dI_{A_{dq\,0}}}{dt}\right) + R_B\left(I_{A_{dq\,0}} - I_{C_{dq\,0}}\right) +$$

$$L_B\left(I_{A_{dq\,0}}K.\frac{dK^{-1}}{dt} + K.K^{-1}\frac{dI_{A_{dq\,0}}}{dt}\right) - L_B\left(I_{C_{dq\,0}}K.\frac{dK^{-1}}{dt} + K.K^{-1}\frac{dI_{C_{dq\,0}}}{dt}\right)\dots\dots\dots\dots\dots\dots(59)$$

$$V_{C_{dq\,0}} = R_A I_{A_{dq\,0}} + L_A(I_{A_{dq\,0}}K.\frac{dK^{-1}}{dt} + \frac{dI_{A_{dq\,0}}}{dt}) + R_B\left(I_{A_{dq\,0}} - I_{C_{dq\,0}}\right) + L_B(I_{A_{dq\,0}}K.\frac{dK^{-1}}{dt} +$$

$$\frac{dI_{A_{dq\,0}}}{dt}) - L_B(I_{C_{dq\,0}}K.\frac{dK^{-1}}{dt} + \frac{dI_{C_{dq\,0}}}{dt}) \dots\dots\dots\dots\dots\dots\dots\dots\dots\dots\dots\dots\dots\dots\dots\dots\dots\dots\dots(60)$$

44

$$\begin{bmatrix} V_{Cd} \\ V_{Cq} \\ V_{C0} \end{bmatrix} = \begin{bmatrix} R_A & 0 & 0 \\ 0 & R_A & 0 \\ 0 & 0 & R_A \end{bmatrix} \begin{bmatrix} I_{A_d} \\ I_{A_q} \\ I_{A_0} \end{bmatrix} + \begin{bmatrix} L_A & 0 & 0 \\ 0 & L_A & 0 \\ 0 & 0 & L_A \end{bmatrix} \begin{bmatrix} 0 & -\omega & 0 \\ \omega & 0 & 0 \\ 0 & 0 & 0 \end{bmatrix} \begin{bmatrix} I_{A_d} \\ I_{A_q} \\ I_{A_0} \end{bmatrix} +$$

$$\begin{bmatrix} L_A & 0 & 0 \\ 0 & L_A & 0 \\ 0 & 0 & L_A \end{bmatrix} \frac{d}{dt} \begin{bmatrix} I_{A_d} \\ I_{A_q} \\ I_{A_0} \end{bmatrix} + \begin{bmatrix} R_B & 0 & 0 \\ 0 & R_B & 0 \\ 0 & 0 & R_B \end{bmatrix} \begin{bmatrix} I_{A_d} \\ I_{A_q} \\ I_{A_0} \end{bmatrix} - \begin{bmatrix} R_B & 0 & 0 \\ 0 & R_B & 0 \\ 0 & 0 & R_B \end{bmatrix} \begin{bmatrix} I_{C_d} \\ I_{C_q} \\ I_{C_0} \end{bmatrix} +$$

$$\begin{bmatrix} L_B & 0 & 0 \\ 0 & L_B & 0 \\ 0 & 0 & L_B \end{bmatrix} \begin{bmatrix} 0 & -\omega & 0 \\ \omega & 0 & 0 \\ 0 & 0 & 0 \end{bmatrix} \begin{bmatrix} I_{A_d} \\ I_{A_q} \\ I_{A_0} \end{bmatrix} + \begin{bmatrix} L_B & 0 & 0 \\ 0 & L_B & 0 \\ 0 & 0 & L_B \end{bmatrix} \frac{d}{dt} \begin{bmatrix} I_{A_d} \\ I_{A_q} \\ I_{A_0} \end{bmatrix} - \begin{bmatrix} L_B & 0 & 0 \\ 0 & L_B & 0 \\ 0 & 0 & L_B \end{bmatrix}$$

$$\begin{bmatrix} 0 & -\omega & 0 \\ \omega & 0 & 0 \\ 0 & 0 & 0 \end{bmatrix} \begin{bmatrix} I_{C_d} \\ I_{C_q} \\ I_{C_0} \end{bmatrix} - \begin{bmatrix} L_B & 0 & 0 \\ 0 & L_B & 0 \\ 0 & 0 & L_B \end{bmatrix} \frac{d}{dt} \begin{bmatrix} I_{C_d} \\ I_{C_q} \\ I_{C_0} \end{bmatrix}$$

$$V_{Cd} = R_A I_d - L_A I_q + L_A \frac{dI_d}{dt} + R_B I_d - R_B I_{C_d} - L_B I_q + L_B \frac{dI_d}{dt} + L_B I_{C_q} - L_B \frac{dI_{C_d}}{dt} \ldots\ldots\ldots(61)$$

After re arrange the previous equation the result is equation (32)

$$(L_A + L_B) \frac{dI_d}{dt} - L_B \frac{dI_{C_d}}{dt} = V_{Cd} - (R_A + R_B) I_d + R_B I_{C_d} + (L_A + L_B) I_q - L_B I_{C_q} \ldots\ldots\ldots(62)$$

$$V_{Cq} = R_A I_q + L_A I_d + L_A \frac{dI_q}{dt} + R_B I_q - R_B I_{C_q} + L_B I_d + L_B \frac{dI_q}{dt} - L_B I_{C_d} - L_B \frac{dI_{C_q}}{dt} \ldots\ldots\ldots(63)$$

After re arrange the previous equation the result is equation (34)

$$(L_A + L_B) \frac{dI_q}{dt} - L_B \frac{dI_{C_q}}{dt} = V_{Cq} - (R_A + R_B) I_q + R_B I_{C_q} - (L_A + L_B) I_d - L_B I_{C_d} \ldots\ldots\ldots(64)$$

Apply KVL around the loop from branches B and C ending with infinite bus

$$0 - V_{inf} \angle \delta_{\text{inf}} = -R_B I_{B_{abc}} - L_B \frac{dI_{B_{abc}}}{dt} + R_C I_{C_{abc}} + L_C \frac{dI_{C_{abc}}}{dt} \dots\dots\dots\dots\dots\dots\dots\dots(65)$$

But $I_{B_{abc}} = I_{A_{abc}} - I_{C_{abc}}$ ....(66)

After substituting I_{Babc} in the previous equation above

$$0 - V_{inf} \angle \delta_{\text{inf}} = -R_B(I_{A_{abc}} - I_{C_{abc}}) - L_B(\frac{dI_{A_{abc}}}{dt} - \frac{dI_{C_{abc}}}{dt}) + R_C I_{C_{abc}} + L_C \frac{dI_{C_{abc}}}{dt} \dots\dots(67)$$

Substituting each abc variable to its dq0 equivalent by multiplying both sides by K^{-1}

$$0 - K^{-1}V_{\text{inf}} \angle \delta_{\text{inf}} = -R_B K^{-1}(I_{A_{dq\,0}} - I_{C_{dq\,0}}) - L_B(\frac{dK^{-1}I_{A_{dq\,0}}}{dt} - \frac{dK^{-1}I_{C_{dq\,0}}}{dt}) +$$

$$R_C K^{-1}I_{C_{dq\,0}} + L_C \frac{dK^{-1}I_{C_{dq\,0}}}{dt} \dots\dots\dots\dots\dots\dots\dots\dots\dots\dots\dots\dots\dots\dots\dots\dots\dots\dots\dots\dots(68)$$

Multiply both sides by K to eliminate the K^{-1} from the left side

$$0 - K.K^{-1}V_{inf} \angle \delta_{\text{inf}} = -R_B K.K^{-1}(I_{A_{dq\,0}} - I_{C_{dq\,0}}) - L_B(K.\frac{dK^{-1}I_{A_{dq\,0}}}{dt} - K.\frac{dK^{-1}I_{C_{dq\,0}}}{dt}) +$$

$$R_C K.K^{-1}I_{C_{dq\,0}} + L_C K.\frac{dK^{-1}I_{C_{dq\,0}}}{dt} \dots\dots\dots\dots\dots\dots\dots\dots\dots\dots\dots\dots\dots\dots\dots\dots\dots(69)$$

$$0 - V_{inf} \angle \delta_{\text{inf}} = -R_B\left(I_{A_{dq\,0}} - I_{C_{dq\,0}}\right) - L_B K.\frac{dK^{-1}I_{A_{dq\,0}}}{dt} + L_B K.\frac{dK^{-1}I_{C_{dq\,0}}}{dt} + R_C I_{C_{dq\,0}} +$$

$$L_C K.\frac{dK^{-1}I_{C_{dq\,0}}}{dt} \dots\dots\dots\dots\dots\dots\dots\dots\dots\dots\dots\dots\dots\dots\dots\dots\dots\dots\dots\dots\dots\dots\dots\dots(69)$$

by derivations the right side and rearrange equations and substituting the park

transformation matrices

46

$$0 - V_{inf} \angle \delta_{inf} = -R_B I_{A_{dq\,0}} + R_B I_{C_{dq\,0}} + L_B (I_{A_{dq\,0}} K.\frac{dK^{-1}}{dt} + K.K^{-1}\frac{dI_{A_{dq\,0}}}{dt}) +$$

$$L_B (I_{C_{dq\,0}} K.\frac{dK^{-1}}{dt} + K.K^{-1}\frac{dI_{C_{dq\,0}}}{dt}) + R_C I_{C_{dq\,0}} + L_C (I_{C_{dq\,0}} K.\frac{dK^{-1}}{dt} + K.K^{-1}\frac{dI_{C_{dq\,0}}}{dt}) \dots\dots(70)$$

$$0 - V_{inf} \angle \delta_{inf} = -R_B I_{A_{dq\,0}} + R_B I_{C_{dq\,0}} + L_B (I_{A_{dq\,0}} K.\frac{dK^{-1}}{dt} + \frac{dI_{A_{dq\,0}}}{dt}) + L_B (I_{C_{dq\,0}} K.\frac{dK^{-1}}{dt} +$$

$$\frac{dI_{C_{dq\,0}}}{dt}) + R_C I_{C_{dq\,0}} + L_C (I_{C_{dq\,0}} K.\frac{dK^{-1}}{dt} + \frac{dI_{C_{dq\,0}}}{dt})\dots\dots\dots\dots\dots\dots\dots\dots(71)$$

$$0 - V_{inf} \angle \delta_{inf} = - \begin{bmatrix} R_B & 0 & 0 \\ 0 & R_B & 0 \\ 0 & 0 & R_B \end{bmatrix} \begin{bmatrix} I_{A_d} \\ I_{A_q} \\ I_{A_0} \end{bmatrix} + \begin{bmatrix} R_B & 0 & 0 \\ 0 & R_B & 0 \\ 0 & 0 & R_B \end{bmatrix} \begin{bmatrix} I_{C_d} \\ I_{C_q} \\ I_{C_0} \end{bmatrix}$$

$$+ \begin{bmatrix} L_B & 0 & 0 \\ 0 & L_B & 0 \\ 0 & 0 & L_B \end{bmatrix} \begin{bmatrix} 0 & -\omega & 0 \\ \omega & 0 & 0 \\ 0 & 0 & 0 \end{bmatrix} \begin{bmatrix} I_{A_d} \\ I_{A_q} \\ I_{A_0} \end{bmatrix} + \begin{bmatrix} L_B & 0 & 0 \\ 0 & L_B & 0 \\ 0 & 0 & L_B \end{bmatrix} \frac{d}{dt} \begin{bmatrix} I_{A_d} \\ I_{A_q} \\ I_{A_0} \end{bmatrix}$$

$$+ \begin{bmatrix} L_B & 0 & 0 \\ 0 & L_B & 0 \\ 0 & 0 & L_B \end{bmatrix} \begin{bmatrix} 0 & -\omega & 0 \\ \omega & 0 & 0 \\ 0 & 0 & 0 \end{bmatrix} \begin{bmatrix} I_{C_d} \\ I_{C_q} \\ I_{C_0} \end{bmatrix} + \begin{bmatrix} L_B & 0 & 0 \\ 0 & L_B & 0 \\ 0 & 0 & L_B \end{bmatrix} \frac{d}{dt} \begin{bmatrix} I_{C_d} \\ I_{C_q} \\ I_{C_0} \end{bmatrix}$$

$$+ \begin{bmatrix} R_C & 0 & 0 \\ 0 & R_C & 0 \\ 0 & 0 & R_C \end{bmatrix} \begin{bmatrix} I_{C_d} \\ I_{C_q} \\ I_{C_0} \end{bmatrix} + \begin{bmatrix} L_C & 0 & 0 \\ 0 & L_C & 0 \\ 0 & 0 & L_C \end{bmatrix} \begin{bmatrix} 0 & -\omega & 0 \\ \omega & 0 & 0 \\ 0 & 0 & 0 \end{bmatrix} \begin{bmatrix} I_{C_d} \\ I_{C_q} \\ I_{C_0} \end{bmatrix}$$

$$+ \begin{bmatrix} L_C & 0 & 0 \\ 0 & L_C & 0 \\ 0 & 0 & L_C \end{bmatrix} \frac{d}{dt} \begin{bmatrix} I_{C_d} \\ I_{C_q} \\ I_{C_0} \end{bmatrix}$$

$$-L_B \frac{dI_d}{dt} + (L_B + L_C)\frac{dI_{C_d}}{dt} = R_B I_d - (R_B + R_C)I_{C_d} - L_B I_q + (L_B + L_C)I_{C_q} - V_{inf}\sin(\delta_{inf})\dots\dots(72)$$

$$-L_B \frac{dI_q}{dt} + (L_B + L_C)\frac{dI_{C_q}}{dt} = R_B I_q - (R_B + R_C)I_{C_q} + L_B I_d - (L_B + L_C)I_{C_d} - V_{inf}\cos(\delta_{inf})\dots\dots(73)$$

47

By substituting and rearrange equations 62,64,72 and 73 to make each equation has only one derivative parameter they become as:

$$\left(\frac{(L_A + L_B)(L_B + L_C)}{L_B} - L_B\right)\frac{dI_{C_d}}{dt} = V_{Cd} + \left(\frac{R_A(L_A + L_B)}{L_B} - (R_B + R_C)\right)I_d + \left(R_B - \frac{(L_A + L_B)(R_B + R_C)}{L_B}\right)I_{C_d} +$$

$$\left(\frac{(L_A + L_B)(L_B + L_C)}{L_B} - L_B\right)I_{C_q} \quad ....(74)$$

$$\left(\frac{(L_A + L_B)(L_B + L_C)}{L_B} - L_B\right)\frac{dI_{C_q}}{dt} = V_{Cq} + \left(\frac{R_A(L_A + L_B)}{L_B} - (R_A + R_B)\right)I_q + \left(R_B - \frac{(L_A + L_B)(R_B + R_C)}{L_B}\right)I_{C_q} +$$

$$\left(L_B - \frac{(L_A + L_B)(L_B + L_C)}{L_B}\right)I_{C_d} - \frac{(L_A + L_B)}{L_B}V_{inf}\cos(\delta_{inf}) \quad ....(75)$$

$$\left(L_A + L_B - \frac{L_B{}^2}{(L_B + L_C)}\right)\frac{dI_d}{dt} = V_{Cd} + \left(\frac{R_B L_B}{L_B + L_C} - (R_A + R_B)\right)I_d + \left((L_A + L_B) - \frac{L_B{}^2}{L_B + L_C}\right)I_q + \left(R_B - \frac{L_B(R_B + R_C)}{L_B + L_C}\right)I_{C_d}...(76)$$

$$\left(L_A + L_B - \frac{L_B{}^2}{(L_B + L_C)}\right)\frac{dI_q}{dt} = V_{Cq} + \left(\frac{L_B{}^2}{L_B + L_C} - (L_A + L_B)\right)I_d + \left(\frac{R_B L_B}{L_B + L_C} - (R_A + R_B)\right)I_q + \left(R_B - \frac{L_B(R_B + R_C)}{L_B + L_C}\right)I_{Cq}...(77)$$

From equations 51 ,52 ,61 and 63 ,the delta angle for PV generator bus during fault is:

$$\tan(\delta_{PV}) = \frac{-LI_{q_{PV}} + V_{Cd}}{LI_{d_{PV}} + V_{Cq}} = \frac{-LI_{q_{PV}} + (R_A + R_B)I_d - R_B I_{C_d} - (L_A + L_B)I_q + L_B I_{C_q}}{LI_{d_{PV}} + (R_A + R_B)I_q - R_B I_{C_q} + (L_A + L_B)I_d - L_B I_{C_d}}...............................(78)$$

48

4.4 Mathematical Model of the System for the Post Fault Running Conditions:

The derivation of the nonlinear dynamical mathematical equations for the system under study at post -fault. The Fault has been cleared by simultaneous opening circuit breaker for the faulted line at two ends.
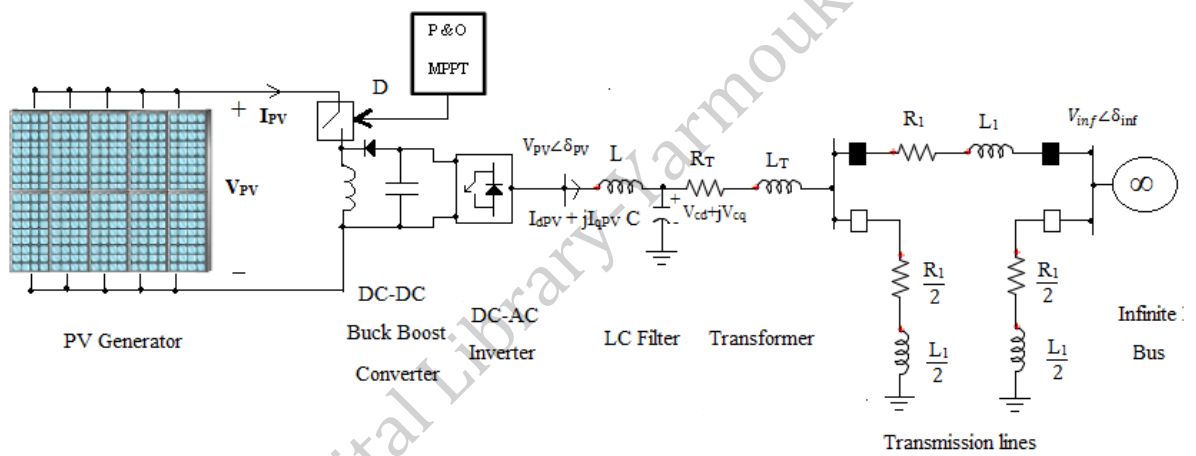

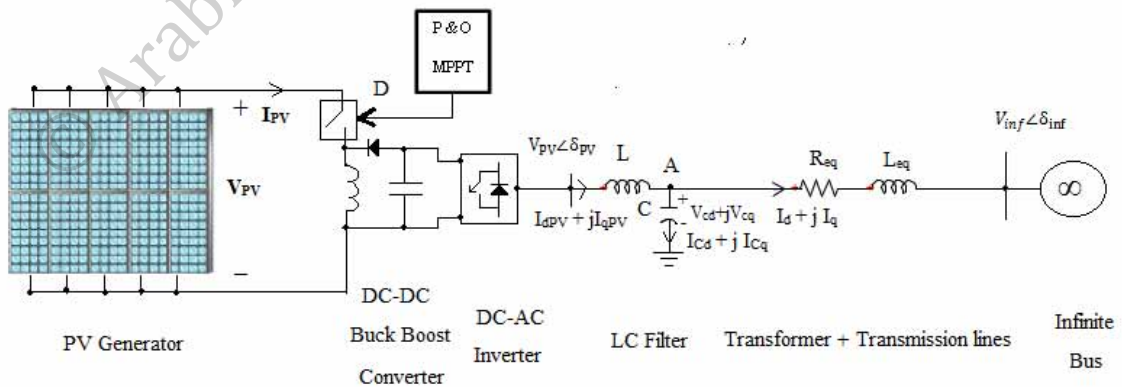Fig.4.7.Schematic diagram for the post fault power system under study

Fig.4.8.Simplified schematic diagram for the post fault power system under study

Equations (79)-(85) represent the mathematical model of the system post fault running conditions. Since the fault has been cleared by tripping the faulted line by opening the two circuit breakers at two ends, so the equivalent system return to its pre-fault running condition except the faulted line tripped and the values of R_{eq} and L_{eq} is increased.

$$C\frac{dV_{Cd}}{dt} = I_{dPV} - I_d + CV_{Cq} \quad\text{..(79)}$$

$$C\frac{dV_{Cq}}{dt} = I_{qPV} - I_q - CV_{Cd} \quad\text{..(80)}$$

$$L\frac{dI_{dPV}}{dt} = \frac{D}{1-D}V_{PV}\sin(\delta_{PV}) + LI_{qPV} - V_{Cd} \quad\text{...................(81)}$$

$$L\frac{dI_{qPV}}{dt} = \frac{D}{1-D}V_{PV}\cos(\delta_{PV}) - LI_{dPV} - V_{Cq} \quad\text{................................(82)}$$

$$L_{eq}\frac{dI_d}{dt} = V_{Cd} - R_{eq}I_d + L_{eq}I_q - V_{inf}\sin(\delta_{inf}) \quad\text{................................(83)}$$

$$L_{eq}\frac{dI_q}{dt} = V_{Cq} - R_{eq}I_q - L_{eq}I_d - V_{inf}\cos(\delta_{inf}) \quad\text{................................(84)}$$

The delta angle for PV generator bus for post fault conditions is:

$$\tan(\delta_{PV}) = \frac{-LI_{qPV} + V_{Cd}}{LI_{dPV} + V_{Cq}} = \frac{-LI_{qPV} + R_{eq}I_d - L_{eq}I_q}{LI_{dPV} + R_{eq}I_q + L_{eq}I_d + V_{inf}\cos(\delta_{inf})} \quad\text{.......................(85)}$$

50

Chapter

5

Chapter 5: Photovoltaic System Design and Perturbation and Observation Algorithm

This chapter presents the design of the photovoltaic generator in actual and per unit quantities at different solar irradiance levels, the area of solar modules and its primary cost. Also it presents the relations between the duty cycle of the DC-DC buck boost converter and its perturbations with the output characteristics of the PV generator based on the P&O algorithm as maximum power point tracking is the target.

5.1 Photovoltaic System Design and Output characteristics

The PV generator consists of many modules connected in parallel and series combinations to achieve the desired values for current , voltage and power. In this thesis, the PV generator design has 548kW$_p$, 471.63 open circuit voltage and 1879.64 A short circuit current. The voltage and current at MPP are 351.71 V&1567A, respectively.In this thesis the PV solar power plant design used the PV module made by AVANCIS Company and designed by PV SOL software.

The PV generator consists of 548 branches and each branch has 8 modules connected in series. The total number of PV modules is 4384 modules. Each module has the following parameter:

52

Table 5.1: I-V characteristic for PV module [23]

I/V Characteristics at STC	
MPP Voltage	43.7 V
MPP Current	2.86 A
Power Rating	125 W
Open Circuit Voltage	58.95 V
Short-Circuit Current	3.43 A
Increase open circuit voltage before stabilization	0 %

The dimension of each module is 664 mm * 1587 mm .So the PV generator surface area is:

PV Module Area is 664 mm * 1587 mm = 1.053 m^2 .

PV Generator Surface = 4384 modules* 1.053m^2/module = 4,619.7 m².

Total Investment Cost=822,000 $ (582565 JOD).

The inverter used in the design is Powador 39,0 TL3manufactured by KACO new energy

and it has the following ratings

DC Power ratings   33.33 kW
AC Power ratings   33.33 kW
Max Input Voltage   1000 V
Max input Current   102 A
Nominal DC Voltage   350 V

So the total number of inverter for the PV solar power plant is 548kWp/33.3kW = **16**

PV Generator Module Area

Name	Area South
PV Modules*	4384 x PowerMax SMART 125 (2013)
Manufacturer	AVANCIS
Inclination	10 °
Orientation	South (180 °)
Installation Type	Mounted - Open Space
PV Generator Surface	4,619.7 m²
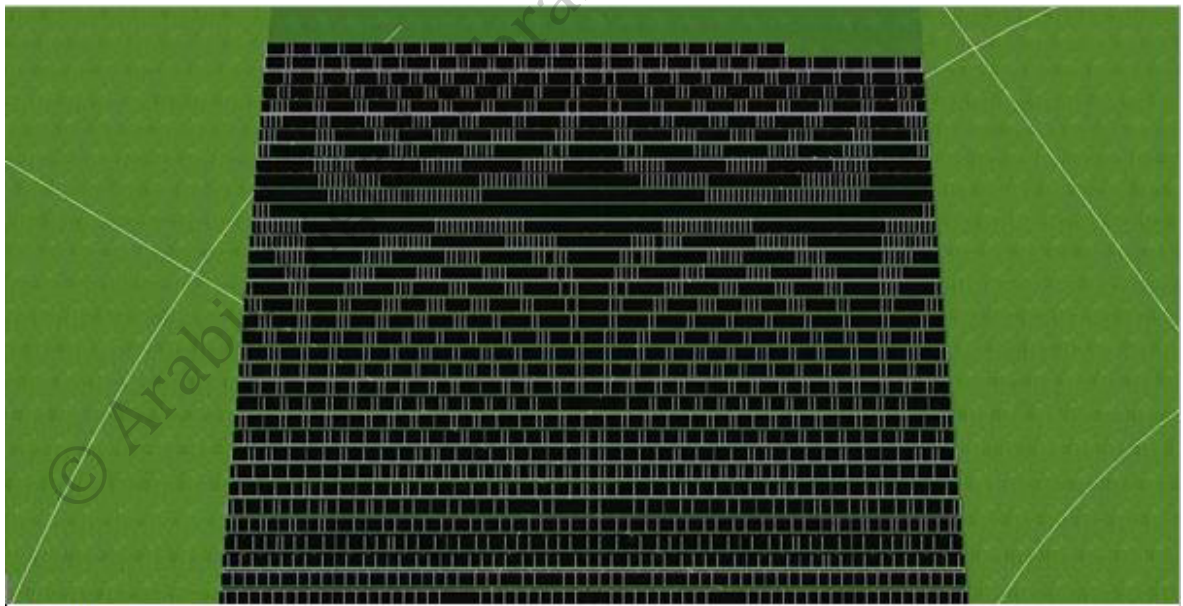
Figure: 3D Design for Area South

Fig.5.1.PV generator design using PV*SOL premium 7.5 (R4) software

54

Figure 5.2 shows the output characteristic for the PV generator Design at full solar irradiance
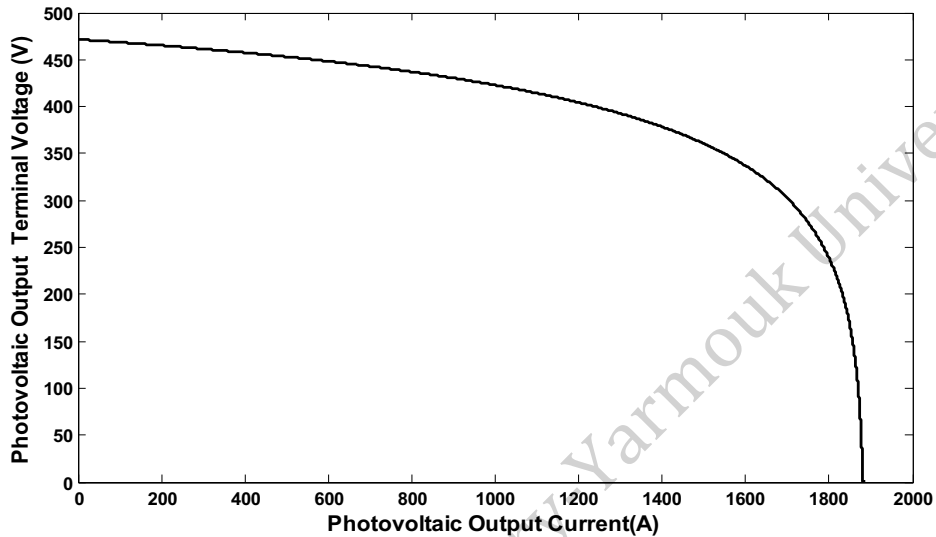
Fig.5.2.Output characteristic for PV generator at full solar irradiance

For more reliable and easy for analysis, the system will be studied in per unit values [21].So choosing 675KVA, 0.4/11 kV transformer as the bases values for all system. The output characteristics for the PV generator in per unit at different solar irradiance levels shown in the Fig .5.3.
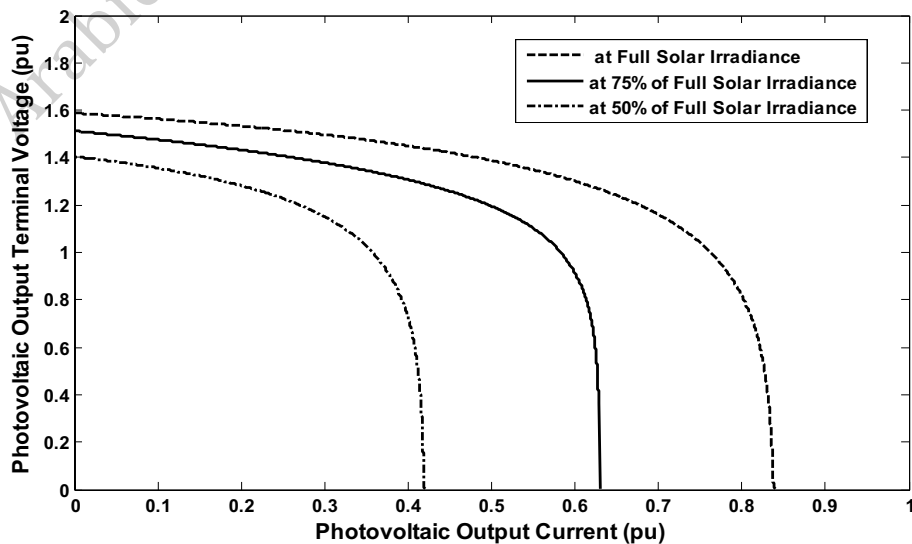

Fig.5.3.Current-voltage characteristics at different solar irradiance levels in per unit

55

The power versus voltage characteristic for PV generator in per unit at different solar   irradiance   levels is shown in Fig.5.4.
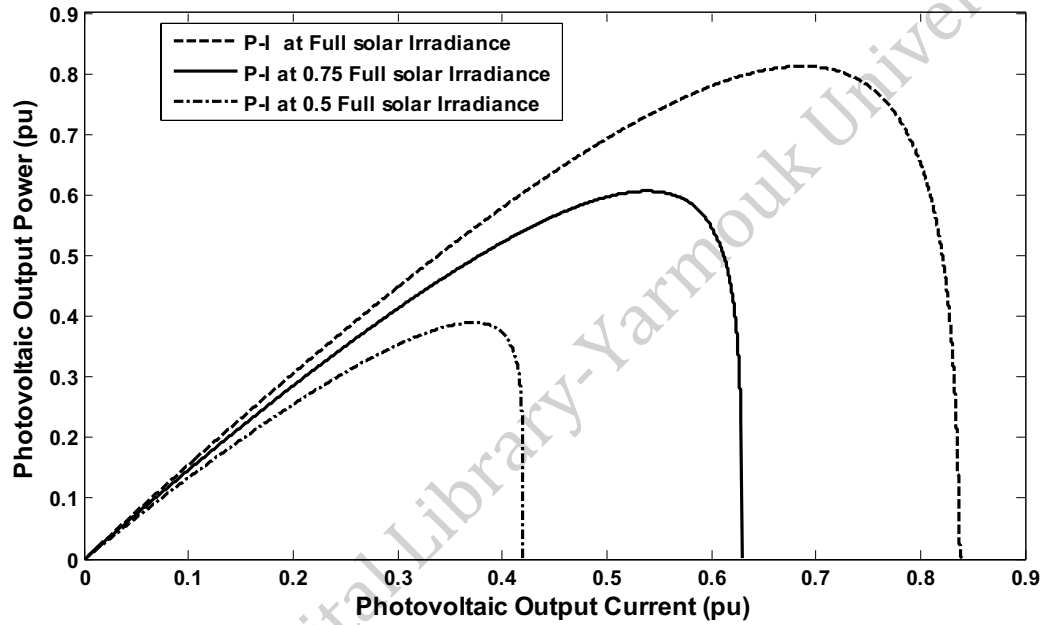
Fig.5.4.Voltage-power relations for PV generator at different solar intensities

From Fig.5.4, the PV generator provides a maximum output power of about 0.812pu at full solar irradiance 0.6089pu at 75% of full solar irradiance and 0.39 pu at 50%offull solar irradiance.

In this thesis, a polynomial of 10th order is used to approximate the nonlinearity of the V-I output characteristics as:

$$V_{PV} = \sum_{n=1}^{11} \alpha_n I_{PV}^{11-n}$$

The constants values for V-I polynomial at different solar irradiance levels are found in appendix A.

56

5.2 Perturbation and Observation algorithm as MPPT technique:

In the P&O algorithm Flow chart in Fig 5.5 ,the values for D and ΔD at corresponding operating point on the output current voltage characteristics are shown in the Fig.5.6 - Fig.5.11 at different solar intensities.
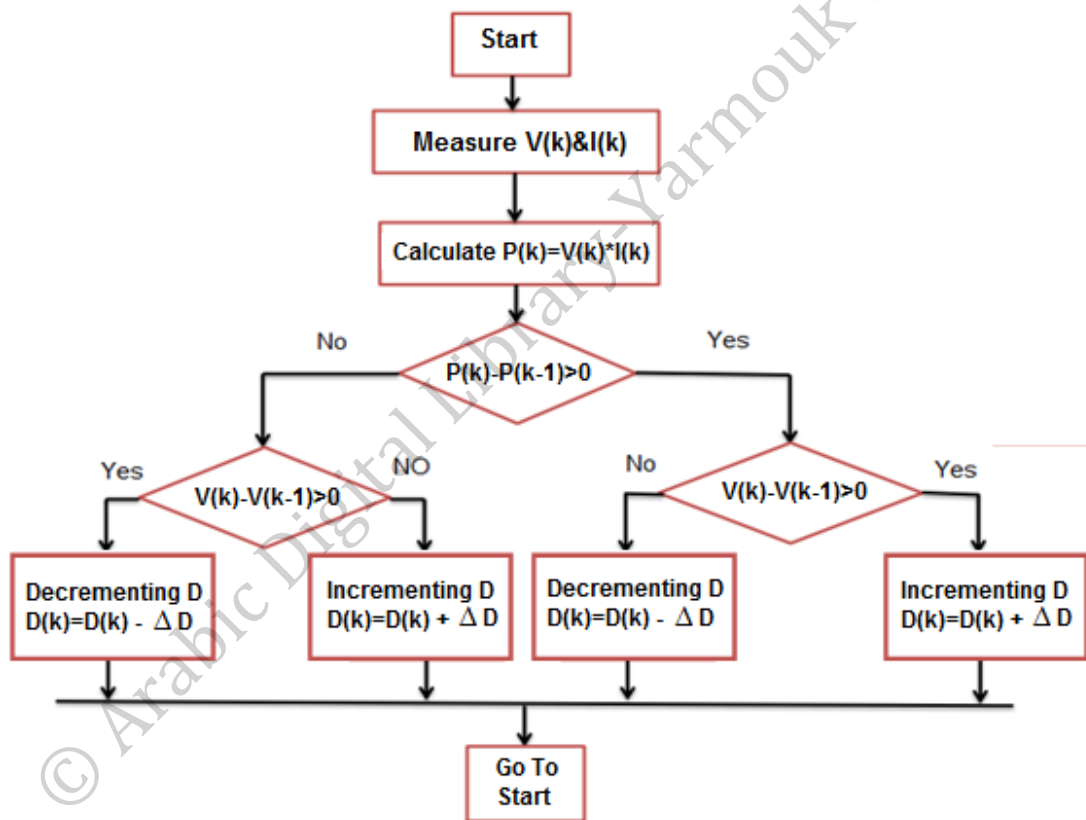

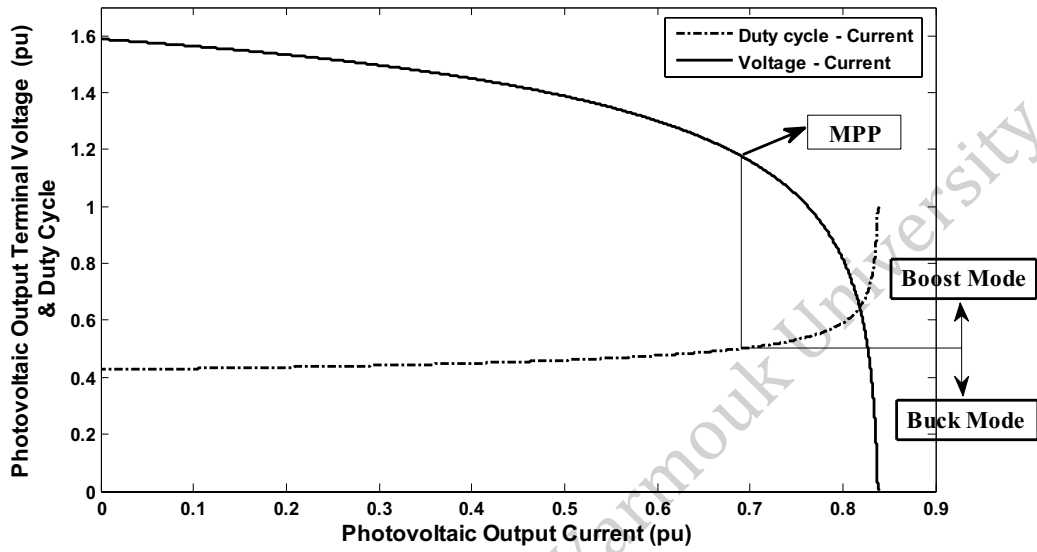Fig.5.5.Flow Chart of P &O algorithm

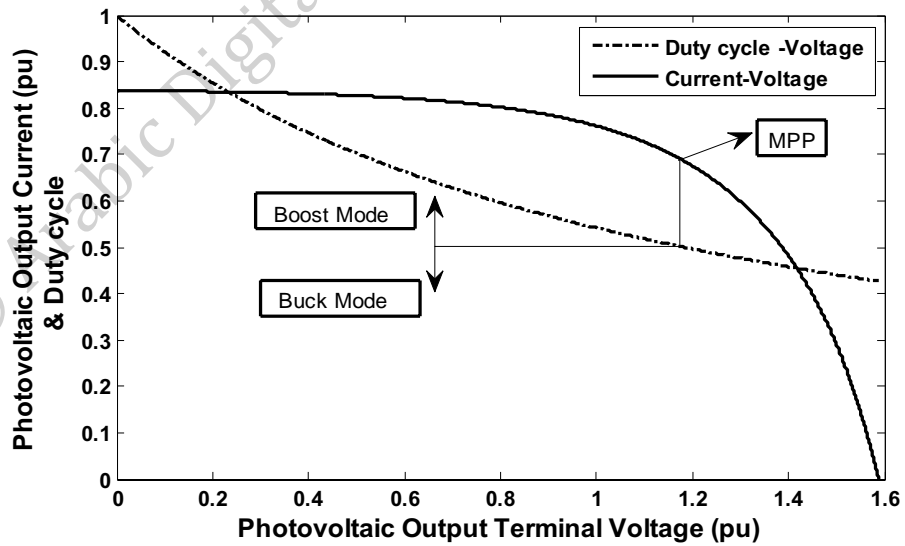Fig.5.6.Duty cycle versus PV current and I-V characteristic based on P&O at full solar irradiance

Fig.5.7. Duty cycle vs. voltage and I-V characteristic based on P&O at full solar irradiance

58
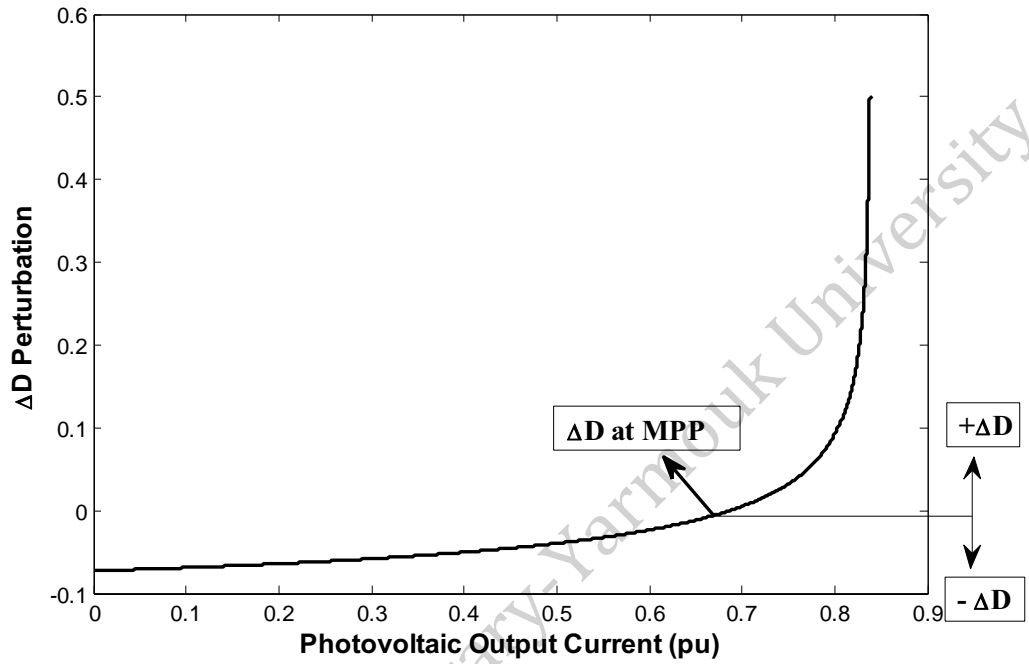
Fig.5.8. Duty cycle perturbation versus PV Current based on P&O algorithm at full solar
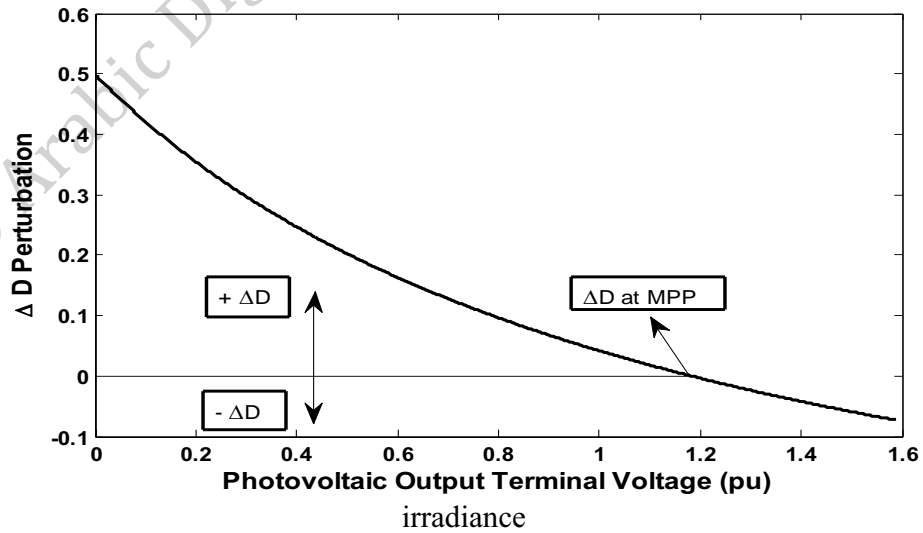

irradiance

Fig.5.9. Duty cycle perturbation versus PV voltage based on P&O algorithm at full solar
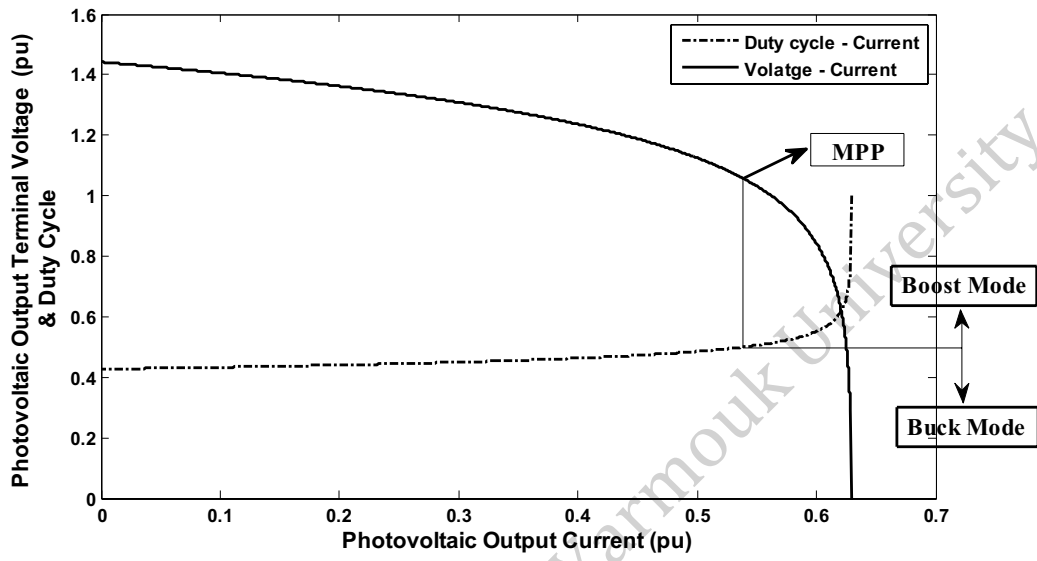irradiance

59

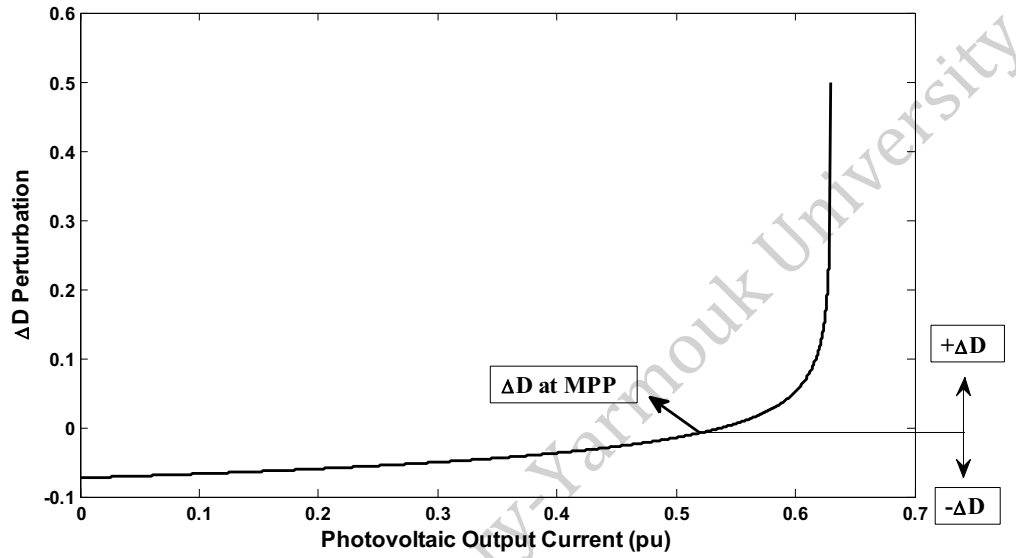Fig.5.10. Duty cycle versus PV current& V-I characteristic based on P&O at 75% of full solar irradiance

Fig.5.11. Duty cycle perturbation versus PV voltage based on P&O algorithm at 75% of full solar irradiance

5.3 System Response After Symmetrical Three Phase to Ground Fault

The numerical simulations of the system after symmetrical three phase to ground fault at the middle of the second transmission line is presented .The fault has been cleared by simultaneous opening the circuit breakers at the faulted line from its two ends . The system behavior during fault case is presented at full solar intensity, 75%, 60% and 50 % of full solar intensity. The system response after successive step changes in the solar irradiance levels from 90% to 75% to 60% and then followed by 100% of full solar irradiance level is presented.

5.3.1 System Response at Full Solar Irradiance Level

Figures 5.12-5.15 show the response of the system when it is subjected to three phase to ground fault which is considered as large disturbance. Three phases to ground fault is subjected at the middle of the second transmission line. A symmetrical three phase to ground fault is occurred for a period of 55 ms .Figure 5.12 shows the output photovoltaic current at pre, during and post fault cases. Figure 5.14 shows the output photovoltaic power at pre, during and post fault cases.

Initially before the fault is affected on the system, the PV generator output power is about 0.812 pu which is corresponding to the maximum output power from the PV generator at full solar irradiance level. The duty cycle for DC to DC converter is about 0.505 which is controlled by the P&O algorithm .The output current is 0.686 pu at output voltage from PV is 1.184 pu.

During the fault the power output from the PV generator is decreased sharply to 0.45 pu. The fault has been cleared by opening the circuit breakers at two ends of the faulted line.

The post fault values for the system is remain within the pre-fault values but still the system need about 5 s to be with a steady state and some oscillation is happened before a steady state values is achieved.
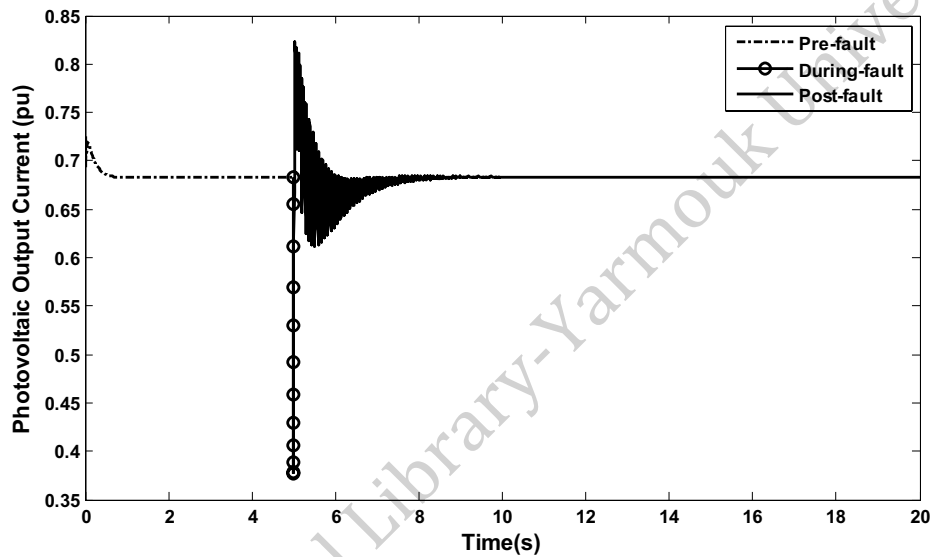

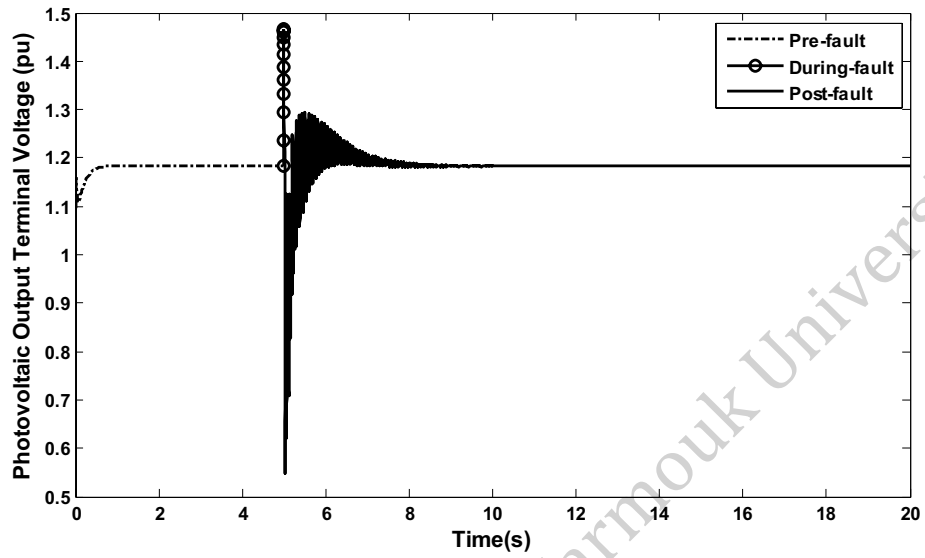Fig.5.12.PV generator output current at full solar irradiance

63

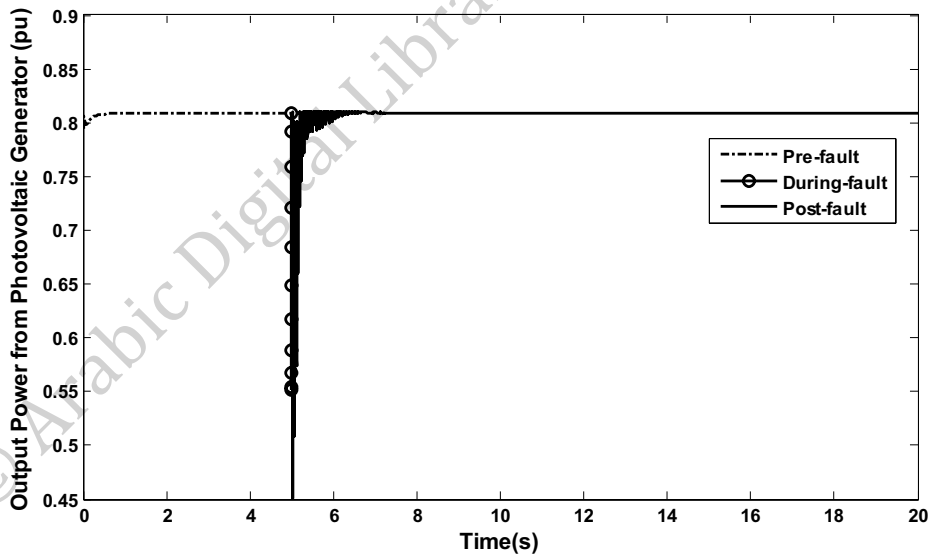Fig.5.13.PV generator injected voltage at full solar irradiance

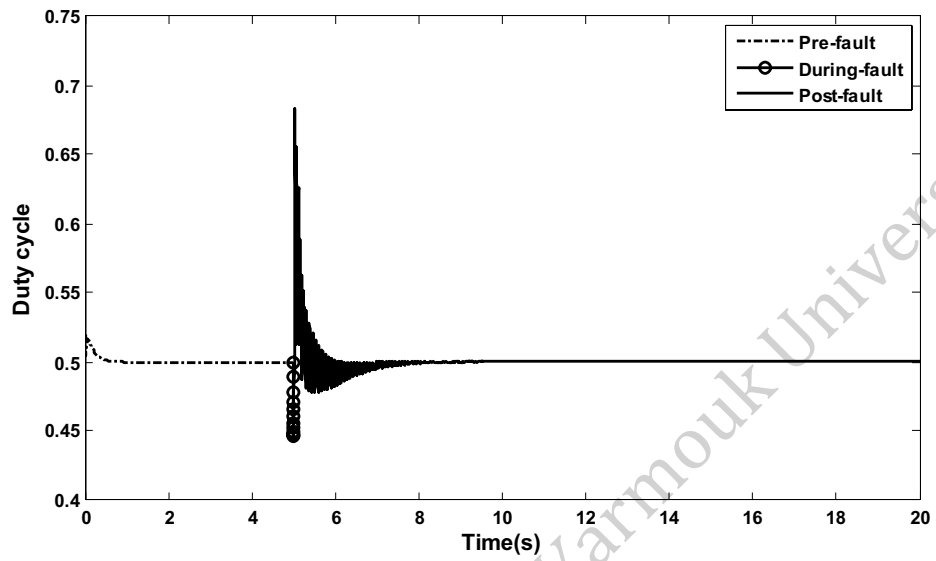Fig.5.14.PV generator output power at full solar irradiance

64

Fig.5.15.Duty cycle for DC-DC converter based on P&O Algorithm

65

5.3.2 System Response at 75% of Full Solar Irradiance Level

Figures 5.16 - 5.19 show the response of the system when it is subjected to three phase to ground fault which is considered as large disturbance. Three phases to ground fault is subjected at the middle of the second transmission line. A symmetrical three phase to ground fault is occurred for a period of 55 ms .Figure 5.16 shows the output photovoltaic current at pre ,during and post fault cases. Figure 5.18 shows the output photovoltaic power at pre ,during and post fault cases.

Initially before the fault is affected on the system, the PV generator output power is about 0.608pu which is corresponding to the maximum output power from the PV generator at 75% of full solar irradiance level. The duty cycle for DC to DC converter is about 0.523 which is controlled by the P&O algorithm .The output current is 0.589 pu at output voltage from PV is 1.047 pu.

During the fault the power output from the PV generator is decreased sharply to 0.58pu. The fault has been cleared by opening the circuit breakers at two ends of the faulted line.

The post fault values for the system remains within the pre-fault values but still the system needs about 80 s to reach steady state and some oscillations taking place before the steady state .
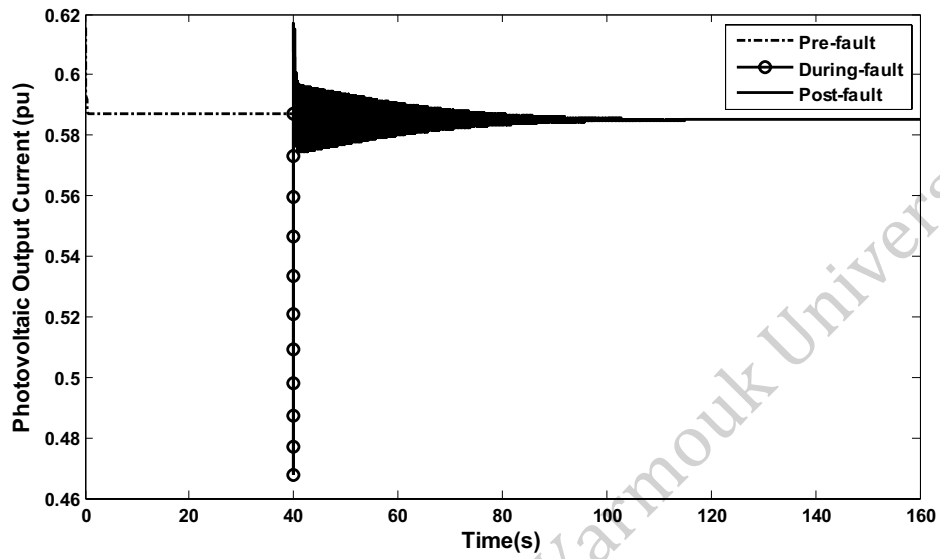
66

Fig.5.16.PV generator output current at 75% of full solar irradiance

Fig.5.17.PV generator injected voltage at 75%of full solar irradiance

© Arabic Digital Library-Yarmouk University

www.manaraa.com

Fig.5.18.PV generator output power at 75% of full solar irradiance
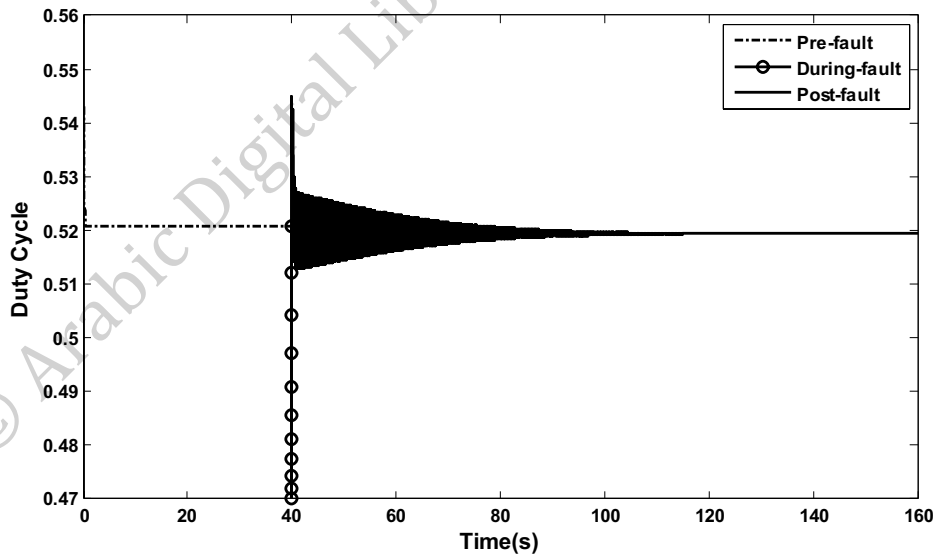
Fig.5.19.Duty cycle for DC-DC converter based on P&O algorithm at 75% of full solar irradiance

68

5.3.3 System Response at 60% of Full Solar Irradiance Level

Figures 5.20 -5.23 show the response of the system when it is subjected to three phase to ground fault which is considered as large disturbance. Three phases to ground fault is subjected at the middle of the second transmission line. A symmetrical three phase to ground fault is occurred for a period of 55 ms . Figure 5.20 shows the output photovoltaic current at pre, during and post fault cases. Figure 5.22 shows the output photovoltaic power at pre, during and post fault cases.

Initially before the fault is affected on the system, the PV generator output power is about 0.435pu which is corresponding to the maximum output power from the PV generator at 60 % of full solar irradiance level. The duty cycle for DC to DC converter is about 0.513 which is controlled by the P&O algorithm .The output current is 0.445 pu at output voltage from PV is 0.983 pu.

During the fault the power output from the PV generator is decreased sharply to 0.421pu. The fault has been cleared by opening the circuit breakers at two ends of the faulted line.

The post fault values for the system is remain within the pre-fault values but still the system need about 190 s to be with a steady state and some oscillation staking place before a steady state is achieved.

69

Fig.5.20.PV generator output current at 60% of full solar irradiance

70

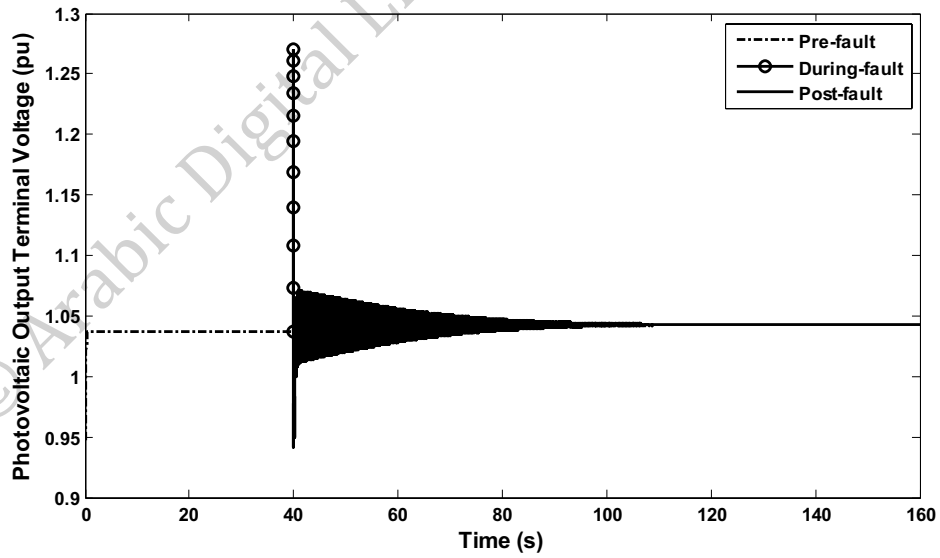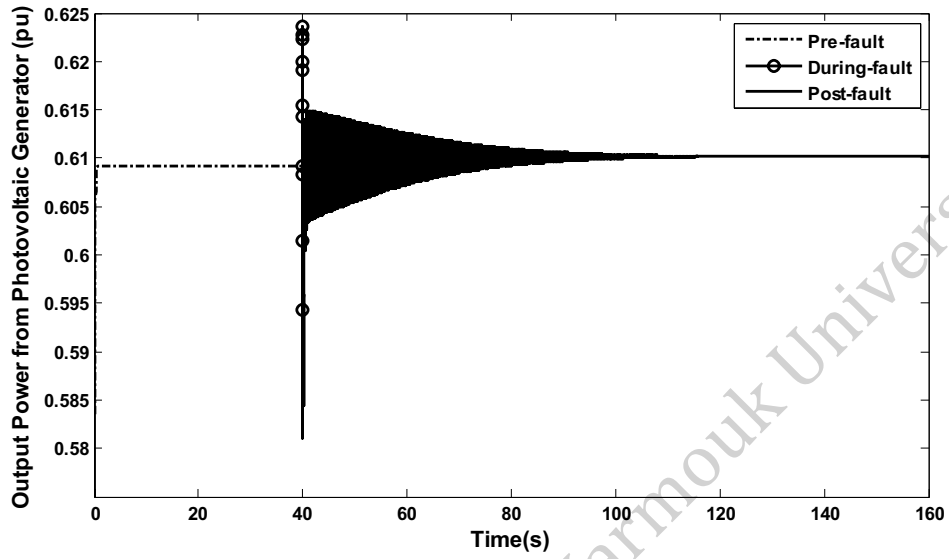Fig.5.21.PV generator injected voltage at 60% of full solar irradiance

Fig.5.22.PV generator output power at 60% of full solar irradiance

71

Fig.5.23.Duty cycle for DC-DC converter based on P&O Algorithm at 60% of full solar irradiance

72

5.3.4 System Response at 50% of Full Solar Irradiance Level

Before the fault is taken place at the middle of second transmission line the system is steady state stable. But the fault affected on the system and its cleared by opening the circuit breaker of the faulted line at two ends. The critical clearing time for the fault is 35 ms which is less than the previous cases to maintain the system in stable operating conditions. The output power from PV generator at pre-fault period is 0.39 which corresponding to the maximum power point which is controlled by P&O algorithm. The output current from PV generator at pre-fault is 0.417 pu and the PV generator injected voltage about 0.949 pu. During the fault, both the output current and output power from PV generator is sharply decreased to 0.28 pu and 0.36 pu respectively. The injected terminal voltage of PV generator is increased sharply during fault to a value of 1.23 pu. After the fault has been cleared. The post fault values for the system is remain within the pre-fault values but still the system need about 210 s to be with a steady state and some oscillations taking place before a steady state is achieved.
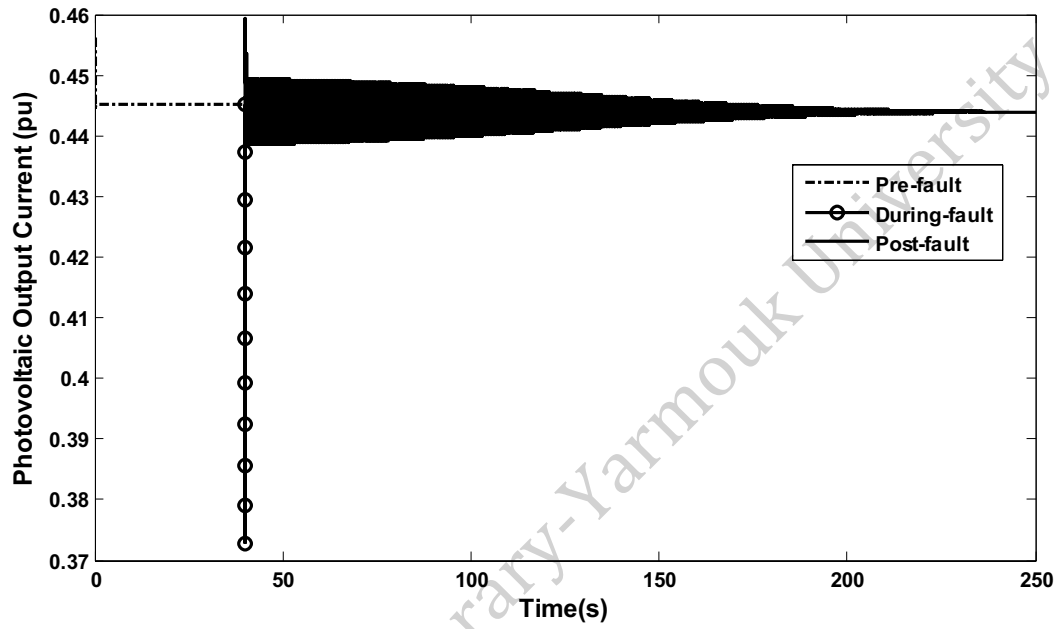
73
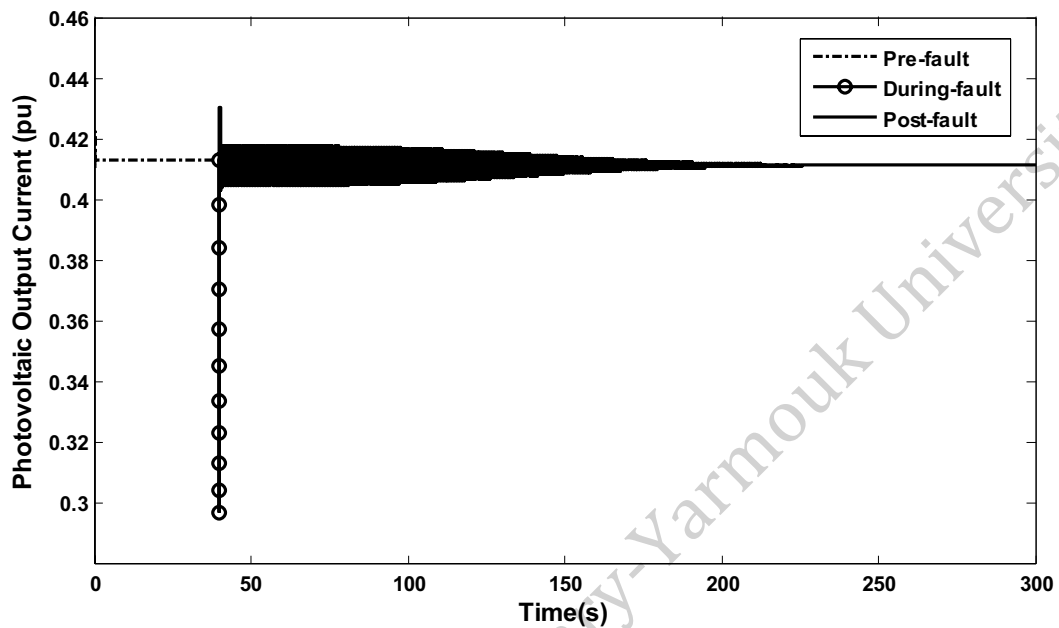
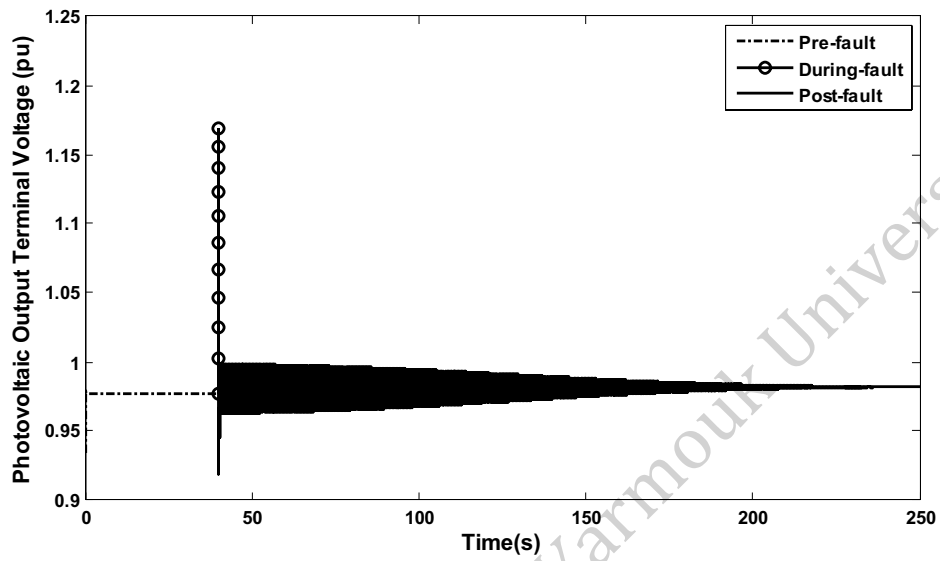Fig.5.24.PV generator output current at 50% of full solar irradiance

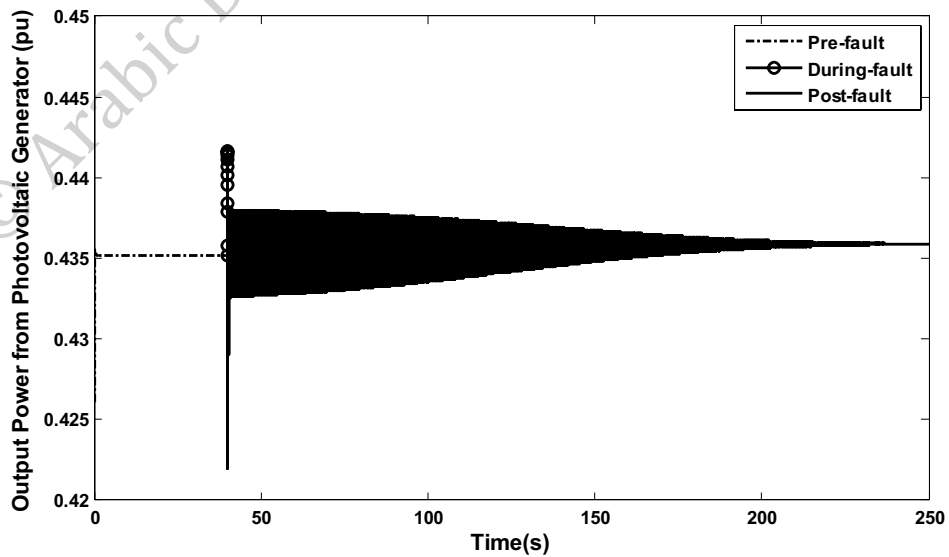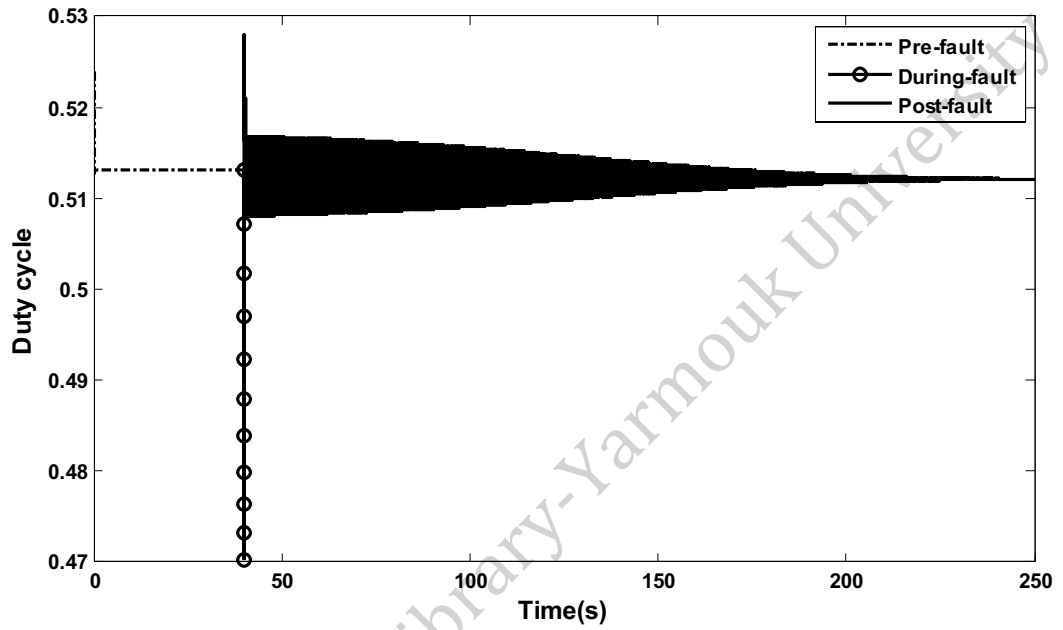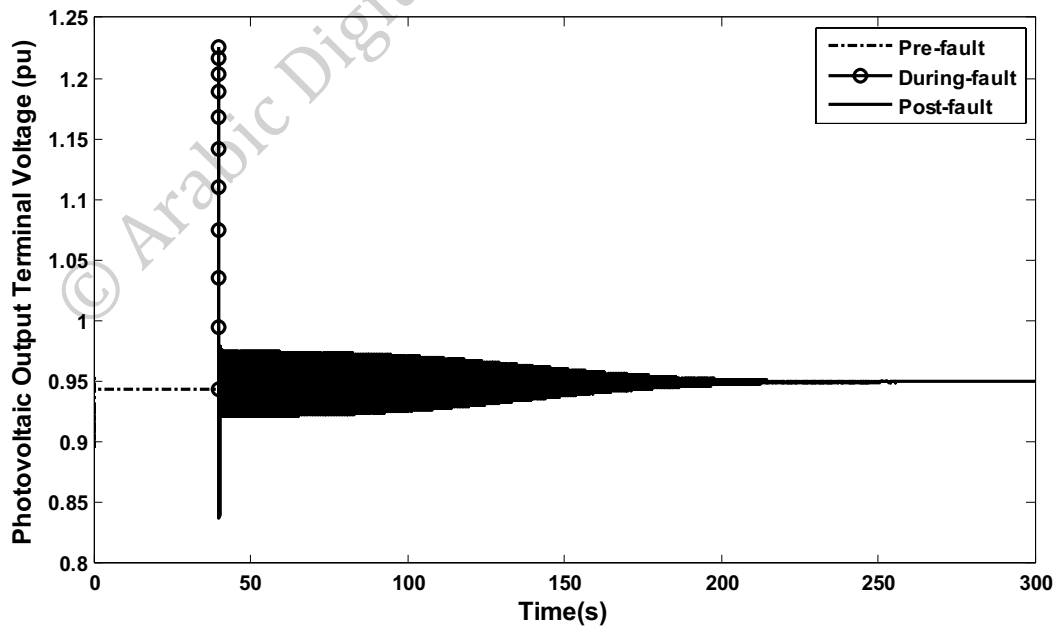Fig.5.25.PV generator injected voltage at 50% of full solar irradiance

74
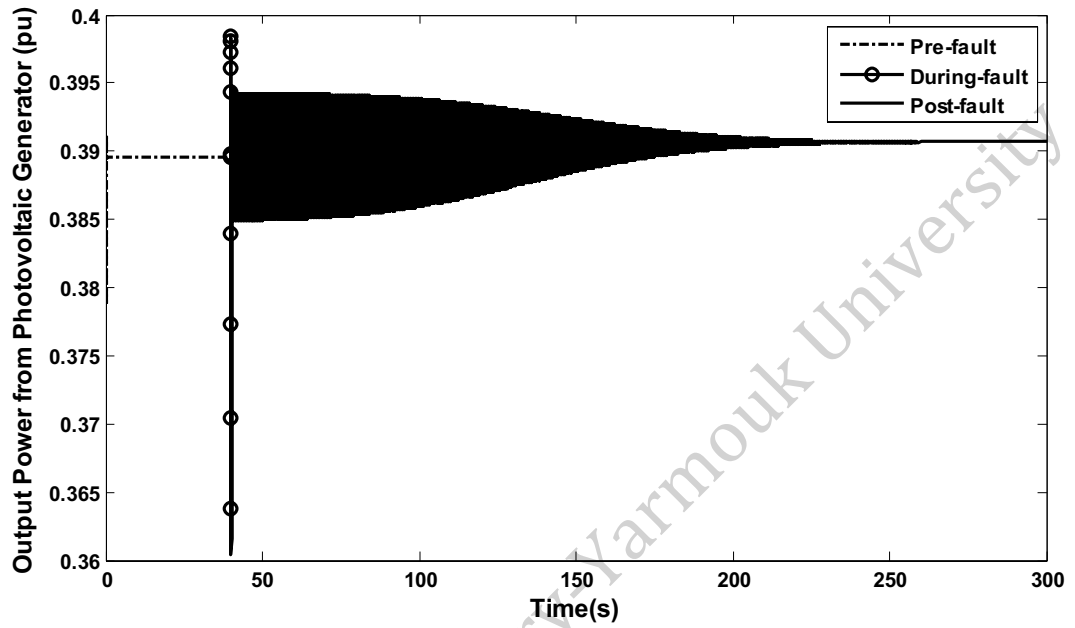
Fig.5.26.PV generator output power at 50% of full solar irradiance
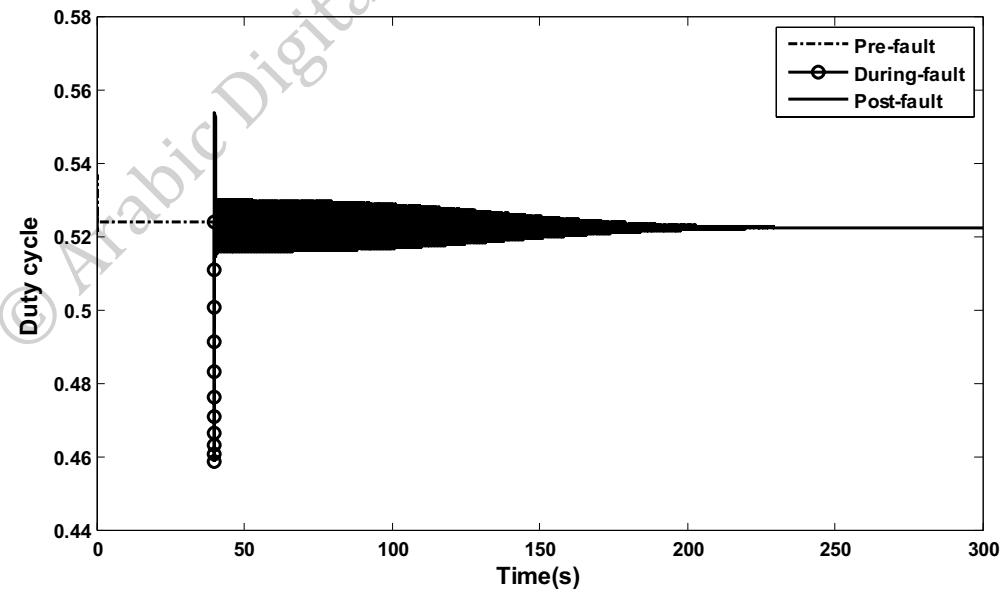
Fig.5.27.Duty cycle for DC-DC converter based on P&O Algorithm at 50% of full solar irradiance

75

5.4 The response of the system after a successive step changes in the solar irradiance levels

Figures 5.28-5.32 show the response of the system after the successive step change in solar irradiance levels of the PV generator from 90% to 75% to 60% and then 100% of full solar intensity.
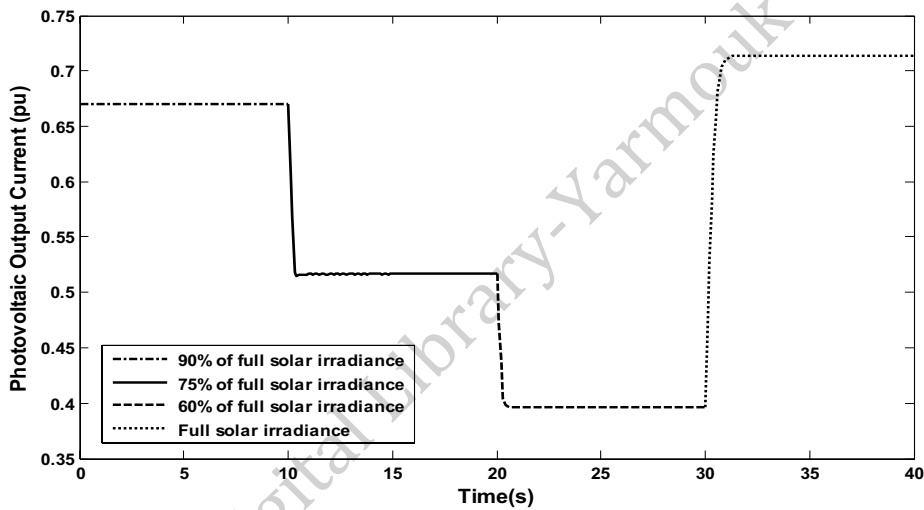
Fig.5.28.PV generator output current at step change of solar intensities
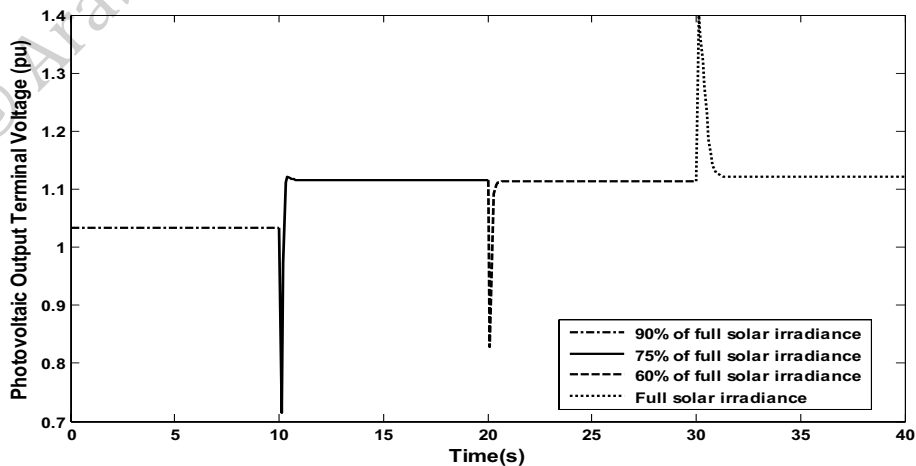
Fig.5.29.PV gnerator injected voltage at step change of solar intensities

76

Figure 5.30 showed that the output power from the PV generator at every solar irradiance level corresponding to the maximum power point of the PV generator of the P-I charateretisc. So the principle of the maximum power point tracking is achieved
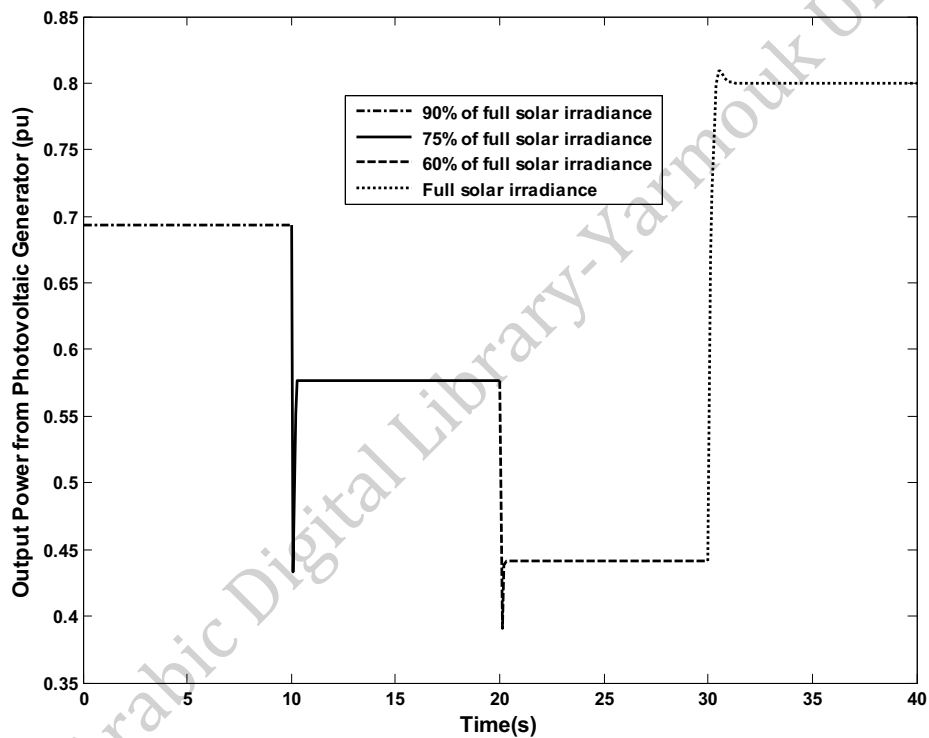
Fig.5.30.PV generator output power at step change of solar intensities

77
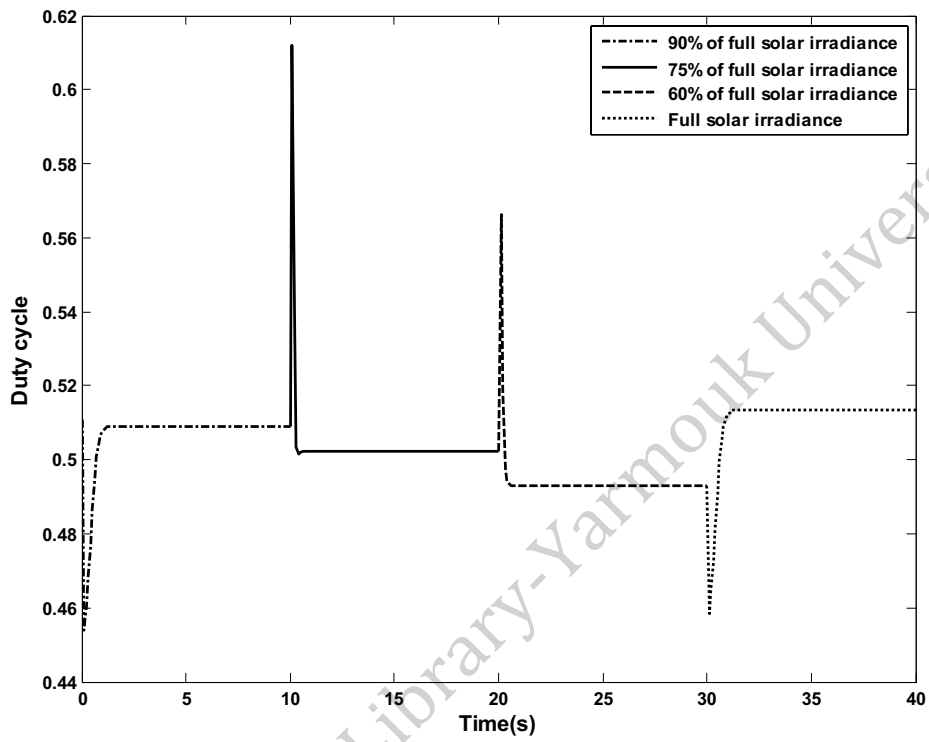
Fig.5.31.Duty cycle for DC-DC converter at step change of solar intensities

78
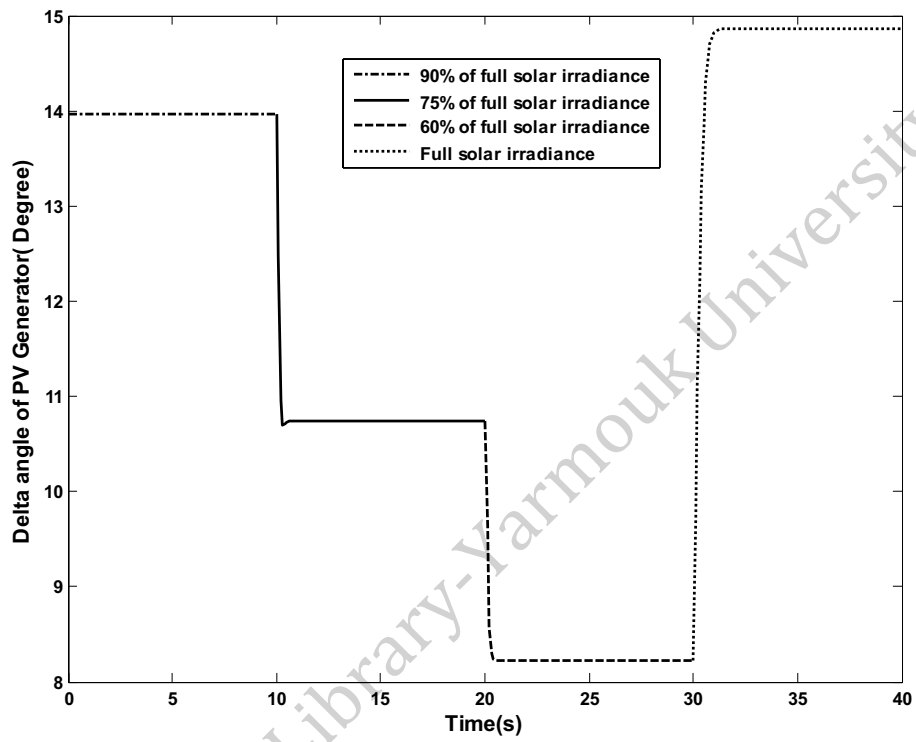
Fig.5.32.PV generator voltage delta angle at step change of solar intensities(Degrees)

79

Chapter

6

Chapter 6 : Conclusion and Future Work

6.1 Conclusion

In this thesis, the perturbation and observation technique as maximum power point tracking techniques is used to track the maximum power of photovoltaic generator integrated to the grid**.** The system under study is comprised of PV generator connected to infinite bus via DC-DC buck boost convertor, DC-AC Inverter, LC filter and two identical transmission lines.

The large signal stability of the power system after a three phase to ground fault is subjected on the middle of the transmission line at different solar irradiance levels is presented.

The response of the system showed that at full solar intensity the output power is tracked by P&O algorithm at about 0.812 pu at duty cycle 0.505 & PV Injected voltage 1.184pu and output PV current is 0.686 pu. During fault the output power is sharply decreased to about 0.45pu. The system needs 5s to return to its pre-fault values after the fault has been cleared.

At 75% of full solar irradiance level ,the output PV generator power is decreased during fault from its maximum value of 0.608 pu to 0.58 pu . The system needs about 80s to return to steady state values .

At 60% of full solar irradiance level ,the output PV generator power is decreased during fault from its maximum value of 0.435pu to 0.421pu. The system needs about 190s to return to steady state values**.**

81

At 50% of full solar irradiance , the critical clearing time is 35 ms to maintain the system in stable operating conditions after the faulted line is removed. The output power during fault is decreased to 0.36 pu. The system needs 210s to return to steady state values.

It can be observed that, the level of solar intensity affects the stability of the power system. As the PV solar irradiance level decreased, the system needs more time to return to stable operating values after the fault has been cleared by opening the circuit breaker at two ends of the faulted line. So the higher PV solar irradiance level is, more stable and robust system. Table 6.1 summarize the results for critical clearing time and the time require to recover stable operating condition at different soar intensities.

Table 6.1: Critical Clearing Times and Times Required to Recover Stability

Solar Intensity Level	Full Solar Intensity	75% of Full Solar Intensity	60% of Full Solar Intensity	50% of Full Solar Intensity
Critical Clearing Time (ms)	55	55	55	35
Time Required to Recover stability(s)	5	80	190	210

The response of the system after successive step changed of solar irradiance level is presented. The PV solar intensity level is step changed from 90% to 75% to 60% and followed by 100% of full solar irradiance. The output powers from PV generator after successive step changes in solar intensities are 0.695 pu, 0.575 pu,0.435 pu and 0.812 pu

82

www.manaraa.com

,respectively. The PV injected voltages are 1.03 pu, 1.12 pu, 1.118 pu and 1.13 pu ,respectively. The PV output current are 0.675 pu, 0.513 pu, 0.389 pu and 0.718 pu ,respectively. The Duty cycle of DC-DC convertor based on P&O algorithm at step changed of solar intensities are 0.51 , 0.503 , 0.493 and 0.518 , respectively .Table 6.2 summarize the results for the response of the system after successive step changes in solar intensities.

Table 6.2 : Response After Successive Step Changes in Solar Intensities

Successive Step Changes in Solar Intensities	90% of Full Solar Intensity	75% of Full Solar Intensity	60% of Full Solar Intensity	100% of Full Solar Intensity
PV Output Current (pu)	0.675	0.513	0.389	0.718
PV Injected Voltage (pu)	1.03	1.12	1.118	1.13
PV Output Power (pu)	0.695	0.575	0.435	0.812
Duty Cycle of Buck Boost Converter	0.51	0.503	0.493	0.518
PV Generator Voltage Delta Angle (Degrees)	14	10.8	8.2	14.8

6.2 Future Work

1. To use a another MPPT technique and make a comparison study between different MPPT techniques and P&O method in my thesis.

2. To study the steady state stability of the power system around the operating point using the eigen values.

3. To study the response of the system at different types of faults and at different locations in the power system.

84

الملخص باللغة العربية

الاسم : ثائر عمر عادل سويدان.

عنوان الرسالة : الخلايا الكهروضوئية ذات القدرة العالية المدمجة مع أنظمة القدرة الكهربائية مع متتبع القيم القصوى

بإستعمال طريقة الاضطراب والمراقبة.

الدرجة : الماجستير في هندسة القوى الكهربائية.

التاريخ : 2015/8/13م.

الملخص التجريدي

في معظم أنظمة القدرة الكهروضوئية، الحد الأقصى لانتاج القدرة من الخلايا الكهروضوئية هو الهدف. هناك العديد من تقنيات متتبع القيم القصوى (MPPT) مثل: جزء جهد الدائرة المفتوحة (FOCV)، جزء تيار قصر الدائرة(FSCC) ، خوارزمية الاضطراب والمراقبة (P & O) ،خوارزمية تصرف تدريجي(IC)، وتحكم المنطق الضبابي(FLC). في هذه الأطروحة، يتم تطبيق خوارزمية الاضطراب والمراقبة (P&O) لتتبع نقطة القدرة القصوى(MPP) للقدرة الناتجة من مولد الخلايا الكهروضوئية. ويتكون النظام القدرة الكهربائية من مولد الخلايا الكهروضئية المتصلة مع نظام الشبكة الكهربائية عبر محول التيار المستمر الى التيار المستمر ، محول التيار المستمر الى التيار المتغير ثلاثي الطور ، مرشح ، محول قدرة كهربائية ثلاثي الطور ، واثنين من خطوط نقل القدرة الكهربائية . تحليل استقرارية النظام الكهربائي مع مولد الخلايا الكهروضوئية المتوافق مع الشبكة تحقق . ويترافق تحليل النظام في إطار محاور المباشر والتربيع (DQ) ، وبالتالي فإن اشتقاق المعادلات الرياضية الديناميكية غير الخطية للنظام في إطار محاور المباشر والتربيع هي واحدة من الخطوات في عملي. درس استقرار النظام المقترح بعد إخضاعه لخطأ ثلاثي الطور مع الارض وبعد التغييرات المتعاقبة في شدة الاشعاع الشمسي لمولد الخلايا الكهروضوئية . تستخدم خوارزمية الاضطراب والمراقبة للسيطرة والتحكم على قيمة دورة التشغيل في محول التيار المستمر الى التيار المستمر (DC-DC) لإعطاء أقصى قدر لانتاج القدرة الكهربائية من مولد الخلايا الكهروضوئية عن طريق الكشف عن موقع نقطة التشغيل لمولد الخلايا الكهروضوئية والسيطرة على قيمة دورة التشغيل في محول التيار المستمر الى التيار المستمر(DC-DC).

85

References

[1] J. P. Dunlop, Photovoltaic System , 3rd Edition , atp,Inc.,2012.

[2] M.R. Patel, Wind and Solar Power System , CRC Press LLC, 1999.

[3] URL:sunstationscotland.net/TypesOfPVcell.html , online: 2011.

[4] A.M. Abd El-Aal, "Modeling and Simulation of a Photovoltaic Fuel Cell Hybrid System", Dissertation for Dr.-Ing,University of Kassel,Germany, 15 April 2005.

[5] H.S.Rauschenbach. "Solar cell array design handbook", Van Nostrand Reinhold, 1980.

[6] A.S.Hadeed , A.F.Murtaza , A. Noman ,K.E.Addoweesh and M. chiaberge ,"An intelligent control strategy of fractional short circuit current maximum power point tracking technique for photovoltaic applications" Journal of Renewable and Sustainable Energy, vol. 7,no.1, 2015.

[7] T. Esram, P.L. Chapman, "Comparison of Photovoltaic Array Maximum Power Point Tracking Techniques," IEEE Transactions on Energy Conversion, vol. 22, no. 2, pp. 439-449, June 2007.

[8] H.A Sher ,"An intelligent off-line MPPT technique for PV applications" , 2013 IEEE Conference on Systems, Process & Control (ICSPC) , vol., no., pp.316,320, 13-15 Dec. 2013

[9] A.Safari, S.Mekhilef, "Simulation and Hardware Implementation of Incremental Conductance MPPT with Direct Control Method Using Cuk Converter", IEEE Trans, March 2010.

[10] S. Jain, V. Agarwal, "Comparison of the performance of maximum power point tracking schemes applied to single-stage grid-connected photovoltaic systems," Electric Power Applications, IET, vol. 1, no. 5, pp. 753-762, Sept. 2007.

[11] D.P Hohm, M.E Ropp., "Comparative Study of Maximum Power Point Tracking Algorithms Using an Experimental, Programmable, Maximum Power Point Tracking Test Bed". Photovoltaic Specialists Conference, 2000. Conference Record of the Twenty-Eighth IEEE 15-22 Sept. 2000, pp. 1699 – 1702.

[12] N. Mohan, T. M. Undeland and W. P. Robbins, Power Electronics, Converters, Applications and Design, (John Wiley & Sons,Inc.,2003).

[13] M. S. Widyan , "Large-Disturbance Stability of Grid-Integrated Photovoltaic Generator with MPPT" International Symposium on Power Electronics, Electrical Drives, Automation and Motion (SPEEDAM) , pp.334 – 341, 18-20 June 2014.

[14] T. Sahu, T.V. Dixit and R. Kumar "Simulation and Analysis of Perturb and Observe MPPT Algorithm for PV Array Using ĊUK Converter" AEEE ISSN 2231-1297, Vol. 4, No. 2 ,pp. 213-224, 2014.

[15] M.Sivagamasundari, P.Melba and M.Velvizhi "Maximum Power Point Tracking For Photovoltaic System by Perturb and Observe Method Using Buck Boost Converter" International Journal of Advanced Research in Electrical, Electronics and Instrumentation Engineering Vol.2, , June 2013.

[16] M. S. Widyan and R. E. Hanitsch , "Operating Point Stability Analysis of SMIB Power System Equipped with High PV Penetration", International Journal of Electrical Power and Energy Systems, Vol. 55, pp. 522-530, 2014.

[17] J. S. Kumari ,C. Sai Babu and A. KamalakarBabu , "Design and Analysis of P&O and IP&O MPPT Techniques for Photovoltaic System ", International Journal of Modern Engineering Research, Vol.2, pp-2174-2180, July-Aug. 2012.

[18] A. P. Yadav , S.Thirumaliah, and G.Haritha , " Comparison of MPPT Algorithms for DC-DC Converters Based PV Systems", International Journal of Advanced Research in Electrical, Electronics and Instrumentation Engineering ,Vol. 1, July, 2012 .

[19] S. Kolsi, H. Samet and M. Ben Amar , "Design Analysis of DC-DC Converters Connected to a Photovoltaic Generator and Controlled by MPPT for Optimal Energy Transfer throughout a Clear Day'' Journal of Power and Energy Engineering, 2014, 2, 27-34.

[20] R.Sridhar, S.Dhar and S.Dash, "Performance analysis of a standalone PV system with reduced switch cascaded multilevel inverter", International Journal of Power and Energy Conversion, Vol.6, No.2 , pp.107 – 127 ,2015.

[21] M.S.Widyan," Large and Small Signal Stability Performance of a Power System Incorporated with PV Generator", International Journal of Power and Energy Systems, Vol. 33, No. 4, pp. 1-9, 2013.

[22] P. Kundur, Power System Stability and Control, New-York, McGraw Hill, Inc.,1993.

[23] URL:www.avancis.de/en/cis-technology/cis-photovoltaics ,Online: 2014.

Appendix

A

Table A.1 presents the numerical system parameters for both pre and post fault running conditions

Table A.1: Numerical System Parameters

Parameters	Value (pu)
R_1	0.0444
R_T	0.0012
L_1	0.44
L_T	0.16
$R_{eq(\text{ Pre-fault})}$	0.0234
$L_{eq(\text{Pre-fault})}$	0.36
$R_{eq \text{ (Post-fault)}}$	0.0456
$L_{eq \text{ (Post-fault)}}$	0.6
$R_{A|}$	0.0123
R_B	0.0056
R_C	0.0111
L_A	0.24
L_B	0.055
L_C	0.11
L	0.01
C	0.015
V_{inf}	1
δ_{inf}	Zero

90

Table A.2: Constants of 10th Order polynomial curve representing Voltage -Current

Characteristics of the PV generator at different solar irradiance levels

Constants	Full solar Intensity	90% of full solar intensity	75% of full solar intensity	60% of full solar intensity	50% of full solar intensity
α_{10}	-33336.615210	-93925.186158	-563524.33871	-5042650.476321	-30182735.5631
α_9	130902.39597	331933.18052	1659587.04125	11880540.813782	59259051.6066
α_8	-218746.85257	-499214.73270	-2079962.55067	-11911917.53289	-49512963.1844
α_7	202806.68286	416553.08158	1446296.14264	6626334.8321643	22952466.9820
α_6	-114028.78549	-210787.61881	-609888.898835	-2235408.328059	-6452553.47901
α_5	39918.030057	66411.334772	160127.747314	469529.31976117	1129421.93760
α_4	-8596.1359999	-12871.195744	-25861.9956638	-60666.38882745	-121607.511229
α_3	1083.3915535	1459.9687890	2444.58681827	4587.5579373325	7663.24256150
α_2	-72.252319806	-87.629923123	-122.273707103	-183.5689241145	-255.534137438
α_1	1.81280083	1.9787605187	2.300872963	2.7634315422596	3.2056583078
α_0	1.57391203	1.5462015855	1.498249924	1.4395618349753	1.391610174

91

Appendix

B

Table B.1: PV Module Data Sheet

Manufacturer	AVANCIS
Available	Yes
Electrical Data	
Cell Type	CIS
Only Transformer Inverters suitable	No
Number of Cells	104
Number of Bypass Diodes	1
Mechanical Data	
Width	664 mm
Height	1587 mm
Depth	37 mm
Frame Width	25 mm
Weight	16 kg
Framed	No
I/V Characteristics at STC	
MPP Voltage	43.7 V
MPP Current	2.86 A
Power Rating	125 W
Open Circuit Voltage	58.95 V
Short-Circuit Current	3.43 A
Increase open circuit voltage before stabilisation	0 %
I/V Part Load Characteristics	
Values source	Manufacturer/user-created
Irradiance	300 W/m²
Voltage in MPP at Part Load	42.7 V
Current in MPP at Part Load	0.86 A
Open Circuit Voltage (Part Load)	54.1 V
Short Circuit Current at Part Load	0.98 A
Further	
Voltage Coefficient	-170 mV/K
Electricity Coefficient	0.1 mA/K
Output Coefficient	-0.39 %/K
Incident Angle Modifier	97 %
Maximum System Voltage	1000 V
Spec. Heat Capacity	920 J/(kg*K)
Absorption Coefficient	70 %
Emissions Coefficient	85 %

Table B.2: Inverter Data Sheet

Manufacturer	KACO new energy
Available	Yes
Electrical Data	
DC Power Rating	33.3 kW
AC Power Rating	33.3 kW
Max. DC Power	39 kW
Max. AC Power	33.3 kW
Stand-by Consumption	30 W
Night Consumption	7 W
Feed-in from	120 W
Max. Input Current	102 A
Max. Input Voltage	1000 V
Nom. DC Voltage	350 V
Number of Feed-in Phases	3
Number of DC Inlets	4
With Transformer	No
Change in Efficiency when Input Voltage deviates from Rated Voltage	-0.5 %/100V
MPP Tracker	
Output Range < 20% of Power Rating	99.4 %
Output Range > 20% of Power Rating	99.6 %
No. of MPP Trackers	3
Max. Input Current per MPP Tracker	34 A
Max. recommended Input Power per MPP Tracker	20 kW
Min. MPP Voltage	200 V
Max. MPP Voltage	800 V

94